VYSOKÉ UČENÍ TECHNICKÉ V BRNĚ
BRNO UNIVERSITY OF TECHNOLOGY

FAKULTA INFORMAČNÍCH TECHNOLOGIÍ
ÚSTAV POČÍTAČOVÉ GRAFIKY A MULTIMÉDIÍ

FACULTY OF INFORMATION TECHNOLOGY
DEPARTMENT OF COMPUTER GRAPHICS AND MULTIMEDIA

ODHAD LETOVÝCH PARAMETRŮ MALÉHO LETOUNU

LIGHT AIRPLANE FLIGHT PARAMETERS ESTIMATION

ROZŠÍŘENÝ ABSTRAKT DISERTAČNÍ PRÁCE
EXTENDED ABSTRACT OF PHD THESIS

AUTOR PRÁCE Ing. PETR DITTRICH
AUTHOR

VEDOUCÍ PRÁCE Ing. PETER CHUDÝ, Ph.D. MBA
SUPERVISOR

BRNO 2016

Abstract

This thesis is focused on a light airplane flight parameter estimation, specially aimed at the Evektor SportStar RTC. For the purposes of flight parameter estimation the Equation Error Method, Output Error Method and Recursive Least–Squares methods were used. This thesis is focused on the investigation of the characteristics of the flight parameters of longitudinal motion and the verification, that this estimated parameters corresponds to the measured data and thus create a prerecquisite for a sufficiently accurate airplane model. The estimated flight parameters are compared to the a–priori values obtained using the Tornado, AVL and Datcom softwares. The differences between the a–priori values and estimated flight parameters are also compared to the correction factors published for the subsonic flight regime of an F–18 Hornet model.

Keywords

Airplane, System Identification, Parameter Estimation, Flight Parameters, Flight Envelope, Equations of Motion, Linearization, State–Space Model, Longitudinal Motion, Equation Error Method, Output Error Method, Recursive Least–Squares, Sensors, Flight Path Reconstruction, Kalman Filter, Model Validation.

Citation

Petr Dittrich: Light airplane flight parameters estimation, Extended abstract of PhD thesis, Brno, BUT FIT, 2016

Abstrakt

Tato práce je zaměřena na odhad letových parametrů malého letounu, konkrétně letounu Evektor SportStar RTC. Pro odhad letových parametrů jsou použity metody “Equation Error Method”, “Output Error Method” a metody rekurzivních nejmenších čtverců. Práce je zaměřena na zkoumání charakteristik aerodynamických parametrů podélného pohybu a ověření, zda takto odhadnuté letové parametry odpovídají naměřeným datům a tudíž vytvářejí předpoklad pro realizaci dostatečně přesného modelu letadla. Odhadnuté letové parametry jsou dále porovnávány s a–priorními hodnotami získanými s využitím programů Tornado, AVL a softwarovéverze sbírky Datcom. Rozdíly mezi a–priorními hodnotami a odhadnutými letovými paramatery jsou porovnány s korekcemi publikovanými pro subsonické letové podmínky modelu letounu F–18 Hornet.

Klíčová slova

Letoun, identifikace systému, odhad parametrů, letové parametry, letová obálka, pohybové rovnice, linearizace, stavový model, podélný pohyb, “Equation Error Method”, “Output Error Method”, rekurzivní nejmenší čtverce, senzory, rekonstrukce letové trajektorie, Kálmánův filtr, validace modelu.

Citace

Petr Dittrich: Odhad letových parametrů malého letounu, rozšířený abstrakt disertační práce, Brno, FIT VUT v Brně, 2016

Light airplane flight parameters estimation

Declaration

I hereby declare that this thesis is my genuine work, created under the guidance of my supervisor Assistant professor Peter Chudý. All information sources and publications used are properly cited.

. . . .
Petr Dittrich
August 29$^{\text{th}}$, 2016

Acknowledgment

I would like to thank my supervisor Assistant professor Peter Chudý for his guidance and valuable comments on my research work. I also would like to thank my family, my friends and my colleagues at Faculty of Information Technology, Brno University of Technology for their support.

Contents

1. Introduction

In 2009, Federal Aviation Administration (FAA) conducted a study regarding the safety of Light Sport Airplanes (LSA) [15] in the USA. They have discovered that the LSA has over 2.5 times higher fatal accidents rate than the CS[1]–23 airplanes. During the investigated period, 39 fatal LSA accidents were observed, 54% were due to the loss of control, 10% were due to the structural failure. To decrease the high fatal accident rate of LSA, it seems to be necessary to increase the pilot awareness and to reduce pilots' workload during all phases of flight.

The estimation of the flight parameters and building a high fidelity model of the airplane enables manufacturing of build a flight simulators, which will be able to match the behavior of the real airplane more precisely and therefore improve pilot training. The estimated flight parameters are also the prerequisites in design of an advanced 4–axis autopilot, which can lower pilots' workload during the flight.

Moreover, knowledge of the flight parameters can be useful during the development of new airplane to verify the validity of the design within the flight envelope and to enable to focus the tests on specific points of the flight envelope.

Another major application of the identified aircraft model is the aircraft certification process, as the identified model can be used to investigate the stability point. The dynamic stability is one of the requirements of the EASA (European Aviation Safety Agency) Certification Standards, e.g., CS–23 paragraph 181, CS–25 paragraph 181 and CS–VLA[2] paragraph 181.

Due to the existence of a large amount of flight parameters, the author has decided to focus on the estimation of the static stability parameters, damping and control derivatives of the longitudinal motion. The input data were recorded during the test flights on an experimental airplane. For the purposes of the flight tests, the flight envelope was limited to the conditions of altitudes, airspeed and position of center of mass, as consulted with the airplane manufacturer. The limits reflect the safety constraints to prevent extreme attitudes.

[1]CS – Certification Specifications
[2]VLA – Very Light Airplane

1.1 Objectives of the thesis

According to the above mentioned facts, the objectives of this Ph.D. thesis were set as follows:

1. Research on the theory of flight data acquisition, flight parameters estimation, including the sensors used in avionics and Equations of Motion, respectively.
2. Selection of algorithms suitable for the flight parameters estimation of a light airplane.
3. Implementation of selected algorithms and evaluation of the results including proposals for future work.

In the evaluation of the results, following main research questions are addressed:

1. Do the flight parameters of the longitudinal motion fall within the range of values expected for this category of airplanes?
2. Do the force coefficients contained in the above mentioned flight parameters of longitudinal motion exhibit linear behavior for the investigated part of the flight envelope?
3. Do the estimated flight parameters describe sufficiently the airplane aerodynamics? Do, therefore, the simulated flight data based on the estimated flight parameters sufficiently correspond to the measured flight data?
4. What are the correction factors between the a–priori data and their refined values obtained using the parameter estimation methods on the basis of the measured flight data?
5. Are the above mentioned corrections similar to other categories of airplanes?

2. Modeling

In this chapter, it is necessary to describe the modeling behind the identification process, i.e., mostly kinematics and dynamics of motion, and present the used notation. Because of a large amount of theory, only parts needed as a theoretical background for this thesis are presented. Notation introduced in this thesis is based on standards ISO[1] 80000-1:2009 [20] and ISO 80000-2:2009 [21].

Firstly, kinematics of translational and rotational motion, e.g., positions, velocity and acceleration, is described. Secondly, rigid body dynamics, e.g., force and moment of force, is given. Thirdly, the airplane subsystems modeling is presented. Fourthly, the nonlinear Equations of Motion are composed and split into symmetric and antisymmetric equations. Fifthly, the linearization process and the resultant linear Equations of Motion are described.

2.1 Kinematic model

The kinematics describes the motion of an object without the consideration of its mass and forces acting on it. The kinematic model can be divided into two parts: kinematics of the translational motion and the kinematics of the rotational motion.

2.1.1 Kinematics of translational motion

First of all, it is necessary to describe the position of an object and then proceed its velocity and acceleration.

Positions in aerospace applications are often specified in a Cartesian coordinate system using metric length units. [11, 29].

$$\vec{r}_{Xf} = \begin{bmatrix} x \\ y \\ z \end{bmatrix}_{Xf} \tag{2.1}$$

where x, y, z are the positions along particular axes and X is the arbitrary point.

Translational velocity describes the change of position in time and is given in meters per second [11, 41]. Translational velocity $\vec{v}_{Gf}$ of the aircraft's center of mass G relative to the general reference frame F_f is defined in the following term:

$$\frac{\mathrm{d}\vec{r}_{Gf}}{\mathrm{d}t} = \begin{bmatrix} \dot{x} \\ \dot{y} \\ \dot{z} \end{bmatrix}_{Gf} \equiv \vec{v}_{Gf} = \begin{bmatrix} u \\ v \\ w \end{bmatrix}_{Gf} \tag{2.2}$$

where u, v, w are the translational velocities along particular axes.

[1] ISO – International Organization for Standardization

The translational velocity can also be expressed using the transformation from the Geodetic coordinate system to the Geodetic reference frame in a Cartesian coordinate system as specified in the following term [1, 41]:

$$\vec{v}_{Xo} = \begin{bmatrix} \dot{\varphi}\,(M_0 + h) \\ \dot{\ell}\,(N_0 + h)\cos\varphi \\ -\dot{h} \end{bmatrix}_{Xo} \tag{2.3}$$

where h is the height above the ellipsoid, M_0 is the meridian radius of curvature of the ellipsoid[2], and N_0 is the prime vertical radius of curvature of the ellipsoid. These quantities are given by following equations:

$$M_0 = \frac{a\left(1 - e^2\right)}{\left(1 - e^2\sin^2\varphi\right)^{3/2}} \tag{2.4a}$$

$$N_0 = \frac{a}{\sqrt{1 - e^2\sin^2\varphi}} \tag{2.4b}$$

where a is the semi–major axis of the ellipsoid and e is the first eccentricity of the ellipsoid equal to:

$$e^2 = 2f - f^2 \tag{2.5}$$

where f is the flattening of the ellipsoid.

Aircraft airspeed (the translational velocity of the aircraft's center of mass G, relative to the surrounding air) is usually measured in a Spherical coordinate system. A transformation of the translational velocities at point G in a Spherical coordinate system F_b to Cartesian coordinate system F_b are [25, 41]:

$$u_{Gb} = V\ \cos\beta\ \cos\alpha \tag{2.6a}$$

$$v_{Gb} = V\ \sin\beta \tag{2.6b}$$

$$w_{Gb} = V\ \cos\beta\ \sin\alpha \tag{2.6c}$$

where V is the magnitude of the true airspeed.

On the contrary, an inverse transformation, i.e., translational velocity at point G from a Cartesian coordinate system F_b to a Spherical coordinate system F_b, is determined using following expressions [25, 29]:

$$V = \sqrt{u_{Gb}^2 + v_{Gb}^2 + w_{Gb}^2} \tag{2.7a}$$

$$\alpha = \arctan\frac{w_{Gb}}{u_{Gb}} \tag{2.7b}$$

$$\beta = \arcsin\frac{v_{Gb}}{V} \tag{2.7c}$$

Translational acceleration describes a change of the translational velocity in time and is given in meters per second squared [1, 7]. The translational acceleration $\vec{a}_{Gf}$ at point G relative to the general reference frame F_f is defined as:

$$\frac{\mathrm{d}\vec{v}_{Gf}}{\mathrm{d}t} = \begin{bmatrix} \dot{u} \\ \dot{v} \\ \dot{w} \end{bmatrix}_{Gf} \equiv \vec{a}_{Gf} = \begin{bmatrix} a_x \\ a_y \\ a_z \end{bmatrix}_{Gf} \tag{2.8}$$

[2] For the purposes of this thesis, the WGS84 ellipsoid is used.

where a_x, a_y, a_z are the translational accelerations along particular axes.

The derivative of the airspeed describes the translational acceleration of the aircraft's center of mass relative to the surrounding air. Based on Equations 2.7, the derivative of the aircraft airspeed is defined as follows [25, 41]:

$$\dot{V} = \frac{1}{V}\left(u_{Gb}\,\dot{u}_{Gb} + v_{Gb}\,\dot{v}_{Gb} + w_{Gb}\,\dot{w}_{Gb}\right) \tag{2.9a}$$

$$\dot{\alpha} = \frac{u_{Gb}\,\dot{w}_{Gb} - w_{Gb}\,\dot{u}_{Gb}}{u_{Gb}^2 + w_{Gb}^2} \tag{2.9b}$$

$$\dot{\beta} = \frac{V\dot{v}_{Gb} - v_{Gb}\dot{V}}{V\sqrt{u_{Gb}^2 + w_{Gb}^2}} \tag{2.9c}$$

2.1.2 Kinematics of rotational motion

After the kinematics of the translational motion was described, it is important to introduce physical quantities of the rotational motion, i.e., Euler angles, rotation matrix, angular rates, angular velocity and angular acceleration.

The coordinate rotation of a rigid body in a three–dimensional space is defined using a transformation between the reference frame of a rigid body and the reference frame in which we want to describe rotation [41, 43]. The coordinate rotation can be specified using the Rotation matrix or the Euler angles.

The Euler angles $\vec{\Theta}$ are a sequence of three angles which represents the transformation from one reference frame to another [2, 41]. Each angle represents rotation in particular axis. Rotation order used in the aerospace domain is z-y-x. The transformation from the reference frame F_o to the reference frame F_b using Euler angles vector $\vec{\Theta}_{ob}$ is given [2]:

$$\vec{\Theta}_{ob} = \begin{bmatrix} \phi \\ \theta \\ \psi \end{bmatrix}_{ob} \tag{2.10}$$

where ϕ is the angle of rotation around x-axis (i.e., roll angle or bank angle), θ is the angle of rotation around y-axis (i.e., pitch angle or elevation angle), and ψ is the angle of rotation around z-axis (i.e., yaw angle, heading angle or azimuth angle).

Considering the convention for the aerospace applications [2], the yaw angle ψ can range from $-\pi$ to π, pitch angle θ can range from $-\pi/2$ to $\pi/2$ and roll angle ϕ can range from $-\pi$ to π.

Rotation matrix $\boldsymbol{C}$ (sometimes called the Direction Cosine Matrix) describes the transformation from one reference frame to another frame in the Cartesian coordinate system [38, 41]. Rotation matrix is always orthogonal and its determinant is unity. For example, transformation from the reference frame F_o to the reference frame F_b is given by:

$$\vec{\chi}_b = \boldsymbol{C}_{bo} \cdot \vec{\chi}_o \tag{2.11}$$

where $\vec{\chi}_o$ is the general vector in the reference frame F_o, $\vec{\chi}_b$ is the general vector in the reference frame F_b, and $\boldsymbol{C}_{ob}$ is the rotation matrix from the reference frame F_o to the reference frame F_b.

Rotation matrix $\boldsymbol{C}_{ob}$ for an inverse coordinate rotation (i.e., from reference frame F_b to reference frame F_o) is described using following term [7, 41]:

$$\boldsymbol{C}_{ob} = \boldsymbol{C}_{bo}^{-1} = \boldsymbol{C}_{bo}^{T} \tag{2.12}$$

Rotation matrix $\boldsymbol{C}_{ab}$ used for the computation of two subsequent transformations (i.e., from reference frame F_b to reference frame F_s and then from reference frame F_s to reference frame F_a) can be computed as follows [25, 41].

$$\boldsymbol{C}_{ab} = \boldsymbol{C}_{as} \cdot \boldsymbol{C}_{sb} \tag{2.13}$$

The coordinate transformation in Euler angles can be converted to a rotation matrix, given that coordinate transformation can be divided into three subsequent transformations. The resultant rotation matrix can be created by combining these three rotation matrices [38, 43]:

$$\boldsymbol{C}_{ob} = \boldsymbol{C}_{x}(\phi)\, \boldsymbol{C}_{y}(\theta)\, \boldsymbol{C}_{z}(\psi) \tag{2.14}$$

where $\boldsymbol{C}_{x}(\phi)$ is the rotation matrix around x axis, $\boldsymbol{C}_{y}(\theta)$ is the rotation matrix around y axis, and $\boldsymbol{C}_{z}(\psi)$ is the rotation matrix around z axis, which are equal to:

$$\boldsymbol{C}_{x}(\phi) = \begin{bmatrix} 1 & 0 & 0 \\ 0 & \cos\phi & \sin\phi \\ 0 & -\sin\phi & \cos\phi \end{bmatrix} \tag{2.15a}$$

$$\boldsymbol{C}_{y}(\theta) = \begin{bmatrix} \cos\theta & 0 & -\sin\theta \\ 0 & 1 & 0 \\ \sin\theta & 0 & \cos\theta \end{bmatrix} \tag{2.15b}$$

$$\boldsymbol{C}_{z}(\psi) = \begin{bmatrix} \cos\psi & \sin\psi & 0 \\ -\sin\psi & \cos\psi & 0 \\ 0 & 0 & 1 \end{bmatrix} \tag{2.15c}$$

The resultant rotation matrix $\boldsymbol{C}_{bo}$ is:

$$\boldsymbol{C}_{bo} = \begin{bmatrix} \cos\theta\cos\psi & \cos\theta\sin\psi & -\sin\theta \\ \sin\phi\sin\theta\cos\psi - \cos\phi\sin\psi & \sin\phi\sin\theta\sin\psi + \cos\phi\cos\psi & \sin\phi\cos\theta \\ \cos\phi\sin\theta\cos\psi + \sin\phi\sin\psi & \cos\phi\sin\theta\sin\psi - \sin\phi\cos\psi & \cos\phi\cos\theta \end{bmatrix}_{bo} \tag{2.16}$$

The angular velocity describes the rotation speed from one reference frame to another and is always given in radians per second [11, 41]. The angular velocity $\vec{\omega}_{ob}$ of the reference frame F_o relative to the reference frame F_b is defined in following expression:

$$\vec{\omega}_{ob} = \begin{bmatrix} p \\ q \\ r \end{bmatrix}_{ob} \tag{2.17}$$

where p, q, r are the angular velocities around particular axes, whereby all rotations are simultaneous.

Angular rates, sometimes called the Euler angle rates, describe the change of the Euler angles in time and are given in radians per second [1, 19]. Angular rates $\dot{\vec{\Theta}}_{ob}$ are the time derivatives of the Euler angles of the reference frame F_o relative to the reference frame F_b and are defined as follows:

$$\dot{\vec{\Theta}}_{ob} = \begin{bmatrix} \dot{\phi} \\ \dot{\theta} \\ \dot{\psi} \end{bmatrix}_{ob} \tag{2.18}$$

The transformation of the angular rates to the angular velocities with respect to the Euler angles ranges is defined using following equations [25, 51]:

$$p = \dot{\phi} - \dot{\psi} \sin\theta \tag{2.19a}$$
$$q = \dot{\psi} \cos\theta \sin\phi + \dot{\theta} \cos\phi \tag{2.19b}$$
$$r = \dot{\psi} \cos\theta \cos\phi - \dot{\theta} \sin\phi \tag{2.19c}$$

On the contrary, the transformation from the angular velocities to the angular rates is based on the Equations 2.19, and is given by [25, 29]:

$$\dot{\phi} = p + (q \sin\phi + r \cos\phi) \tan\theta \tag{2.20a}$$
$$\dot{\theta} = q \cos\phi - r \sin\phi \tag{2.20b}$$
$$\dot{\psi} = \frac{q \sin\phi + r \cos\phi}{\cos\theta} \tag{2.20c}$$

Equations 2.20 leads to singularity (similar to Gimbal–lock problem[3]) [**Gimbal**, **Kenwright**], as there is no solution of Equation 2.20c for $\theta = \pm\pi/2$. Gimbal–lock problem can be avoided by using different computation theories (e.g., quaternions [43]).

The angular acceleration describes the change of the angular velocity in time and is given in radians per second squared [19, 41]. The angular acceleration $\vec{\alpha}_{ob}$ of the reference frame F_o relative to the reference frame F_b is defined in following terms:

$$\vec{\alpha}_{ob} = \begin{bmatrix} \dot{p} \\ \dot{q} \\ \dot{r} \end{bmatrix}_{ob} \tag{2.21}$$

Given that some reference frames are rotating relative to others, e.g., reference frame F_b relative to reference frame F_o, it is necessary to adapt some of the above presented equation to this rotation.

The transformation between the general vectors $\vec{\chi}$ in rotating reference frames F_o and F_b is defined as [25, 36]:

$$\frac{\mathrm{d}\vec{\chi}_o}{\mathrm{d}t} = \frac{\mathrm{d}\vec{\chi}_b}{\mathrm{d}t} + \omega_{ob} \times \vec{\chi}_b \tag{2.22}$$

The translational acceleration $\vec{a}_o$, can be calculated in rotating reference frames using two different approaches. The first approach is based on the use of the translational velocity

[3]Gimbal–lock is a phenomenon related to mechanical gimbal, when gimbal system looses a degree of freedom due to parallel configuration of several axes.

vector. Given that the translational acceleration is the first derivative of the translational velocity, the $\vec{a}_o$ can be expressed using Equation 2.22 as:

$$\vec{a}_o = \vec{a}_b + \vec{\omega}_{ob} \times \vec{v}_b \tag{2.23}$$

The second approach is based on the utilization of the position vector. Given that the translational acceleration is the second derivative of the position, the $\vec{a}_o$ can be expressed using Equation 2.22 as:

$$\vec{a}_o = \vec{a}_b + 2\,\vec{\omega}_{ob} \times \vec{v}_b + \vec{\omega}_{ob} \times (\vec{\omega}_{ob} \times \vec{r}_b) + \vec{\alpha}_{ob} \times \vec{r}_b \tag{2.24}$$

2.2 Dynamic model

The dynamic model of the rigid body describes the causes of the motion, i.e., forces and moments of forces acting on the object. The dynamic model can be divided to two parts: dynamic model of the translational motion and dynamic model of the rotational motion.

2.2.1 Dynamics of translational motion

At the beginning, it is necessary to introduce the translational momentum and then proceed with the description of the force and the specific force.

Translational momentum $\vec{p}$ is given in kilogram meters per second. Translational momentum $\vec{p}_{Xf}$ of an object in arbitrary point X relative to the general reference frame F_f is defined as follows [11, 25]:

$$\vec{p}_{Xf} = m \cdot \vec{v}_{Xf} \tag{2.25}$$

where m is the mass of the object.

Force is given in Newtons. Force $\vec{F}_{Xi}$ acting on an object in point X relative to Inertial reference frame F_i is given by [1, 41]:

$$\vec{F}_{Xi} = \frac{\mathrm{d}\vec{p}_{Xi}}{\mathrm{d}t} \quad \Rightarrow \quad \vec{F}_{Xi} = \begin{bmatrix} X \\ Y \\ Z \end{bmatrix}_{Xi} \tag{2.26}$$

where X, Y, Z are the forces acting along particular axes.

According to the Second Newton's laws of motion, sum of external forces on the object in center of mass G is defined as follows [1, 11]:

$$\sum \vec{F}_{Gi} = m \cdot \vec{a}_{Gi} \tag{2.27}$$

Force $\vec{F}_o$ was defined as a first derivative of the translational momentum $\vec{p}_o$, therefore it can be expressed in rotating reference frames using Equation 2.22 as:

$$\vec{F}_o = \frac{\mathrm{d}\vec{p}_b}{\mathrm{d}t} + \vec{\omega}_{ob} \times \vec{p}_b \tag{2.28}$$

Furthermore, the derivative of $\vec{p}_b$ can be substituted with 2.26 followed by 2.27 and $\vec{p}_b$ can be replaced with 2.25. The resultant equation can be written as

$$\vec{F}_o = m\,\vec{a}_b + m\,\vec{\omega}_{ob} \times \vec{v}_b \tag{2.29}$$

The specific force describes non–gravitational force per unit mass and is given in meter per second squared [19]. The specific force $\vec{f}_{Xf}$ acting on an object in point X relative to the general reference frame F_f is defined as follows:

$$\vec{f}_{Xf} = \frac{\vec{F}_{Xf} - \vec{G}_{Xf}}{m} \quad \Rightarrow \quad \vec{f}_{Xf} = \begin{bmatrix} f_x \\ f_y \\ f_z \end{bmatrix}_{Xf} \tag{2.30}$$

where $\vec{G}$ is the gravitational force and f_x, f_y, f_z are the specific forces acting along particular axes.

Based on the definition of the Geodetic reference frame F_o, gravitational force $\vec{G}_b$ acting on an arbitrary object can be expressed as [25]:

$$\vec{G}_b = m\,\boldsymbol{C}_{bo}\,\vec{g}_0 = m\,\boldsymbol{C}_{bo} \begin{bmatrix} 0 \\ 0 \\ G_0 \end{bmatrix}_o \tag{2.31}$$

where $\vec{g}_0$ is the gravitational acceleration and G_0 is the magnitude of the standard acceleration of the free fall. For the purposes of this thesis the magnitude of the standard acceleration of the free fall is equal to $9.80665\,ms^{-2}$.

2.2.2 Dynamics of rotational motion

After the dynamics of the translational motion was described, it is necessary to present physical quantities for the rotational motion, i.e., the angular momentum and the moment of force.

Angular momentum $\vec{h}$ is given in kilogram meters squared per second. Angular momentum $\vec{h}_b$ of an object in Body–fixed reference frame F_b is defined in following term [11, 25]:

$$\vec{h}_b = \boldsymbol{J}_b\,\vec{\omega}_{ib} \tag{2.32}$$

where $\boldsymbol{J}_b$ is the inertia tensor, i.e., tensor of moments of inertia:

$$\boldsymbol{J}_b = \begin{bmatrix} J_x & -J_{xy} & -J_{xz} \\ -J_{xy} & J_y & -J_{yz} \\ -J_{xz} & -J_{yz} & J_z \end{bmatrix}_b \tag{2.33}$$

where J_x, J_y, J_z, J_{xy}, J_{xz} and J_{yz} are the elements of the inertia tensor:

$$J_x = \int \left(y_b^2 + z_b^2\right) \mathrm{d}m \tag{2.34a}$$

$$J_y = \int \left(x_b^2 + z_b^2\right) \mathrm{d}m \tag{2.34b}$$

$$J_z = \int \left(x_b^2 + y_b^2\right) \mathrm{d}m \tag{2.34c}$$

$$J_{xy} = \int x_b \, y_b \, \mathrm{d}m \tag{2.34d}$$

$$J_{xz} = \int x_b \, z_b \, \mathrm{d}m \tag{2.34e}$$

$$J_{yz} = \int y_b \, z_b \, \mathrm{d}m \tag{2.34f}$$

Given that aircraft's plane of symmetry is $x_b z_b$ and center of mass of aircraft is lying on this plane, inertia elements J_{xy} and J_{yz} are equal to zero. Therefore inertia tensor of symmetric aircraft is equal to [11]:

$$\boldsymbol{J}_b = \begin{bmatrix} J_x & 0 & -J_{xz} \\ 0 & J_y & 0 \\ -J_{xz} & 0 & J_z \end{bmatrix}_b \tag{2.35}$$

Moment or moment of force describes a tendency of a force to rotate an object about particular axes. Moment $\vec{\tau}_f$ is given in Newton meters and is defined by [1, 25]:

$$\vec{\tau}_f = \frac{\mathrm{d}\vec{h}_f}{\mathrm{d}t} \quad \Rightarrow \quad \vec{\tau}_f = \begin{bmatrix} L \\ M \\ N \end{bmatrix}_f \tag{2.36}$$

or

$$\vec{\tau}_f = \vec{r}_{Xf} \times \vec{F}_{Xf} \tag{2.37}$$

where L, M, N are the moments of force acting around particular axes, $\vec{r}_{Xf}$ is the vector from the origin of the general reference frame F_f to the point X where the force is applied.

Moment $\vec{\tau}_o$, defined as first derivative of angular momentum $\vec{h}_b$, can be expressed in rotating reference frames using Equation 2.22 as:

$$\vec{\tau}_o = \frac{\mathrm{d}\vec{h}_b}{\mathrm{d}t} + \vec{\omega}_{ob} \times \vec{h}_b \tag{2.38}$$

Moreover, the vector $\vec{h}_b$ can be replaced by Equation 2.32. Given that $\vec{\omega}_{ob} \approx \vec{\omega}_{ib}$, and that the resulting derivative of $\vec{\omega}_{ob}$ can be replaced by Equation 2.21, therefore Equation 2.38 can be rewritten as

$$\vec{\tau}_o = \boldsymbol{J}_b \, \vec{\alpha}_{ob} + \vec{\omega}_{ob} \times \boldsymbol{J}_b \, \vec{\omega}_{ob} \tag{2.39}$$

Applying the Second Newton's laws of motion to the rotational motion, sum of external moments is equal to [1]:

$$\sum \vec{\tau}_f = \boldsymbol{J}_f \, \vec{\alpha}_{if} \tag{2.40}$$

2.3 Aircraft model

Detailed aircraft models introduce the forces and moments caused by different elements of an aircraft. The model of a light airplane, used in this thesis, consists of five main parts:

- Mass and inertia model (see Section 2.3.1);
- Aerodynamic model (see Section 2.3.2);
- Propulsion model (see Section 2.3.3);
- Landing gear reaction model; and
- Structural model.

The landing gear model is describing behavior of airplane during taxiing, take–off and landing. Because taxiing, take–off and landing part of the flight are out of the scope of this thesis, the landing gear model is omitted.

The structural model describes elastic properties of airplane structure. This thesis uses point mass approximation of airplane, so the structural model, is out of the scope of this thesis.

2.3.1 Mass and inertia model

The main purpose of a mass and inertia model is to compute the total mass of an aircraft, position of the center of mass and moment of inertia tensor. The change of inertia and mass during flight is so important, that it is necessary to compute this change continuously during the whole flight [47].

In this thesis, we consider only rigid body aircraft. Elastic body aircraft have to have more complex models of mass, inertia and aerodynamics. The model of an elastic aircraft has to account for structural responses changing of all during the flight.

Mass and position of the center of mass of an aircraft are conventionally measurable on the ground. The total mass m of the aircraft is a sum of all elements: empty aircraft, fuel in fuel tanks, pilot, crew and passengers, cargo and other load [26].

Position of the aircraft center of mass $\vec{r}_G$ can be computed as a weighted mean using following formula:

$$\vec{r}_{Gd} = \frac{\sum_i m_i \cdot \vec{r}_{G_i d}}{m} \tag{2.41}$$

where m_i is the mass of the aircraft element i and $\vec{r}_{G_i d}$ is the position of the center of mass of the i^{th} aircraft element.

The inertia tensor $\boldsymbol{J}$ of an aircraft can be obtained in three different ways. The first option considers an experimental measurement using a special oscillation test rig. However this process is highly demanding in terms of infrastructure, equipment and resources [22].

The second option is the possibility to acquire an inertia tensor of any model by Computer Aided Design (CAD) software [48]. Nevertheless it is impractical to create model of every pilot, every cargo and fuel configuration; however, this approach can be easily used for computation of inertia tensor of empty aircraft.

The third option of how to acquire inertia tensor of the whole aircraft, is thus to be computed based on the inertia tensors of individual parts using parallel axis theorem [11, 16]:

$$J_x = \sum_i \left[J_{x_i} + m_i \left(y_{G_i}^2 + z_{G_i}^2 \right) \right]_b \tag{2.42a}$$

$$J_y = \sum_i \left[J_{y_i} + m_i \left(x_{G_i}^2 + z_{G_i}^2 \right) \right]_b \tag{2.42b}$$

$$J_z = \sum_i \left[J_{z_i} + m_i \left(x_{G_i}^2 + y_{G_i}^2 \right) \right]_b \tag{2.42c}$$

$$J_{xy} = \sum_i \left[J_{xy_i} + m_i \, x_{G_i} \, y_{G_i} \right]_b \tag{2.42d}$$

$$J_{yz} = \sum_i \left[J_{yz_i} + m_i \, y_{G_i} \, z_{G_i} \right]_b \tag{2.42e}$$

$$J_{xz} = \sum_i \left[J_{xz_i} + m_i \, x_{G_i} \, z_{G_i} \right]_b \tag{2.42f}$$

where the inertia tensor of an empty aircraft can be acquired from the manufacturer documentation, inertia tensor of the fuel in the fuel tank can be obtain using simulation result based on the shape of the fuel tank, and the inertia tensor of person on–board can be estimated based on procedures and data in specialised document [17].

2.3.2 Aerodynamic model

For the purposes of this thesis, the most important elements of the aerodynamic model are the aerodynamic force and moment of aerodynamic force along with their respective coefficients, i.e., aerodynamic parameters, because these coefficients can be used to approximate the individual flight parameters.

The aerodynamic force $\vec{F}_A$ is often expressed in different coordinate systems. Mutual dependence of these expressions is given in the following equation [11]:

$$\vec{F}_A = \bar{q}\, S \begin{bmatrix} C_X \\ C_Y \\ C_Z \end{bmatrix}_b = \bar{q}\, S \cdot \boldsymbol{C}_{bs} \begin{bmatrix} -C_D \\ C_Y \\ -C_L \end{bmatrix}_s = \bar{q}\, S \cdot \boldsymbol{C}_{ba} \begin{bmatrix} -C_W \\ C_Q \\ -C_L \end{bmatrix}_a \tag{2.43}$$

where $\bar{q}$ is the instant dynamic pressure; S is the reference wing area; C_X, C_Y, C_Z are the coefficients of the aerodynamic force in F_b; C_D, C_L are the coefficients of the aerodynamic force in F_s; and C_W, C_Q are the coefficients of aerodynamic force in F_a. The instant dynamic pressure can be computed using following equation [28, 41]

$$\bar{q} = \frac{1}{2} \rho V^2 \tag{2.44}$$

where ρ is the air mass density.

Moment of aerodynamic force $\vec{\tau}_A$ calculated in Body–fixed reference frame is [11]:

$$\vec{\tau}_A = \bar{q}\, S \begin{bmatrix} b_w \cdot C_l \\ \bar{c} \cdot C_m \\ b_w \cdot C_n \end{bmatrix}_b \tag{2.45}$$

where b_w is the reference wingspan, $\bar{c}$ is the length of Mean Aerodynamic Chord (MAC), and C_l, C_m, C_n are the moment coefficients of the aerodynamic force in the reference frame F_b.

The aerodynamic parameters can be obtained using force coefficients given in Equation 2.43 and moment coefficients given in Equation 2.45. These coefficients can be approximated with arbitrary accuracy in the vicinity of the trim point using Taylor's theorem [**Hazewinkel**]. The resultant equations are [25, 41]:

$$C_X = C_{X0} + \alpha \cdot C_{X\alpha} + q^* \cdot C_{Xq} + \delta_e \cdot C_{X\delta_e} \tag{2.46a}$$
$$C_Y = C_{Y0} + \beta \cdot C_{Y\beta} + p^* \cdot C_{Yp} + r^* \cdot C_{Yr} + \delta_a \cdot C_{Y\delta_a} + \delta_r \cdot C_{Y\delta_r} \tag{2.46b}$$
$$C_Z = C_{Z0} + \alpha \cdot C_{Z\alpha} + q^* \cdot C_{Zq} + \delta_e \cdot C_{Z\delta_e} \tag{2.46c}$$

$$C_D = C_{D0} + \alpha \cdot C_{D\alpha} + q^* \cdot C_{Dq} + \delta_e \cdot C_{D\delta_e} \tag{2.46d}$$
$$C_L = C_{L0} + \alpha \cdot C_{L\alpha} + q^* \cdot C_{Lq} + \delta_e \cdot C_{L\delta_e} \tag{2.46e}$$

$$C_W = C_{W0} + \alpha \cdot C_{W\alpha} + q^* \cdot C_{Wq} + \delta_e \cdot C_{W\delta_e} \tag{2.46f}$$
$$C_Q = C_{Q0} + \beta \cdot C_{Q\beta} + p^* \cdot C_{Qp} + r^* \cdot C_{Qr} + \delta_a \cdot C_{Q\delta_a} + \delta_r \cdot C_{Q\delta_r} \tag{2.46g}$$

$$C_l = C_{L0} + \beta \cdot C_{l\beta} + p^* \cdot C_{lp} + r^* \cdot C_{lr} + \delta_a \cdot C_{l\delta_a} + \delta_r \cdot C_{l\delta_r} \tag{2.46h}$$
$$C_m = C_{m0} + \alpha \cdot C_{m\alpha} + q^* \cdot C_{mq} + \delta_e \cdot C_{m\delta_e} \tag{2.46i}$$
$$C_n = C_{nb} + \beta \cdot C_{n\beta} + p^* \cdot C_{np} + r^* \cdot C_{nr} + \delta_a \cdot C_{n\delta_a} + \delta_r \cdot C_{n\delta_r} \tag{2.46j}$$

where C_{Ij} is the flight parameter (defined as a derivative of coefficient C_I with respect to j in general), δ_e is the deflection of elevator, δ_a is the antisymmetric aileron deflection, δ_r is the deflection of rudder, and p^*, q^*, r^* are the dimensionless angular velocities defined as:

$$p^* = \frac{p\, b_w}{2\, V} \tag{2.47a}$$
$$q^* = \frac{q\, \bar{c}}{2\, V} \tag{2.47b}$$
$$r^* = \frac{r\, b_w}{2\, V} \tag{2.47c}$$

The aerodynamic force and aerodynamic moment, hence its coefficients and aerodynamic parameters, are included in the Equations of Motion. Values of the aerodynamic parameters are obtained by a parameter estimation process, which is based on utilization of Equations of Motion.

2.3.3 Propulsion model

Given that this thesis deals with a light airplane, the propulsion of an airplane is considered to be based on a single reciprocating 4 stroke combustion engine with a propeller. For the purposes of this thesis, it is not necessary to describe the whole propulsion system in detail, therefore only the fuel inputs, propulsion force and moment due to propulsion force are considered.

Fuel inputs (fuel level and fuel flow) are necessary to compute the center of mass and the tensor of inertia of fuel in fuel tanks, as described in Section 2.3.1.

Propulsion force magnitude F_P can be computed using equation [1]:

$$F_P = C_T\, \rho\, n_P^2\, D_P^4 \tag{2.48}$$

where C_T is the dimensionless output thrust coefficient (specified by the propeller manufacturer), n_P is the propeller's rotational speed in revolutions per second, and D_P is the diameter of the propeller.

The propulsion on most of the airplane acts along the x_b axis, so the propulsion force vector $\vec{F}_{Pb}$ can be constructed as:

$$\vec{F}_P = \begin{bmatrix} F_P \\ 0 \\ 0 \end{bmatrix}_b \tag{2.49}$$

Moment due to the propulsion force can be evaluated considering three assumptions. Firstly, the x_b axis does not pass through the center of the propeller. Secondly, the propeller itself is a rotating mass and therefore it generates moment. Finally, the revolutions of the propeller cannot be considered constant, because the airplane used for the purposes of this thesis has fixed pitch propeller. The resultant moment of the propulsion force can be expressed as [11]:

$$\vec{\tau}_P = \vec{r}_{Pb} \times \vec{F}_P + \vec{\omega}_{ob} \times J_P\,\vec{\omega}_P - J_P\,\vec{\alpha}_P \tag{2.50}$$

and simplified to

$$\vec{\tau}_P = \begin{bmatrix} -J_P\,\dot{\omega}_P \\ F_P\,z_{Pb} + J_P\,r\,\omega_P \\ -F_P\,y_{Pb} - J_P\,q\,\omega_P \end{bmatrix} \tag{2.51}$$

where J_P is the moment of inertia of the propeller. The $\vec{\alpha}_P$ and $\vec{\omega}_P$ are acting only around the x_b axis, therefore their vectors contain only the first component, i.e., $\dot{\omega}_P$ and ω_P respectively, and ω_P is the magnitude of angular velocity of the propeller which can be computed as:

$$\omega_P = 2\pi\,n_P \tag{2.52}$$

2.4 Nonlinear Equations of Motion

The Equations of Motion (EoM) describe the behavior of an aircraft (or physical system in general) as a set of mathematical functions. The nonlinear Equations of Motion can be divided into two types: kinematic equations and dynamic equations. At first, the general nonlinear models are introduced. At second, the nonlinear kinematic Equations of Motion are presented. Then, the description of the merge of the Equations of Motion with the rest of aircraft models and the resultant nonlinear dynamic Equations of Motion are given. At the end of this section, dynamic Equations of Motion are divided into the longitudinal equations, and lateral–directional equations.

2.4.1 General nonlinear dynamic system

A general dynamic system is defined as a system, where the outputs in time t depends on inputs in time t and inputs in some of the previous time moment(s) [3, 5]. In general, dynamic system is defined by Equation 2.53.

$$\dot{\vec{x}} = f\left(\vec{x}, \vec{u}\right) \tag{2.53a}$$

$$\vec{y} = h\left(\vec{x}, \vec{u}\right) \tag{2.53b}$$
$$\vec{x}(0) = \vec{x}_0 \tag{2.53c}$$

where $\vec{x}$ is the state vector; $f\left(\right)$ is the state function; $\vec{u}$ is the input/control vector; $\vec{y}$ is the output vector; $h\left(\right)$ is the output function; and $\vec{x}_0$ is the initial state vector.

2.4.2 Nonlinear kinematic Equations of Motion

Nonlinear kinematic equations of the motion describe motion of an object without describing the reason of motion. There are three main nonlinear kinematic EoM: Attitude equations, Navigation equations and Velocity equations.

Attitude equations represent the rate of change of angular position given by transformation from angular velocities to angular rates. These equations were already introduced in Equations 2.20a – 2.20c, but for the sake of completeness are repeated below:

$$\dot{\phi} = p + \left(q \sin\phi + r \cos\phi\right) \tan\theta \tag{2.54a}$$
$$\dot{\theta} = q \cos\phi - r \sin\phi \tag{2.54b}$$
$$\dot{\psi} = \frac{q \sin\phi + r \cos\phi}{\cos\theta} \tag{2.54c}$$

Navigation equations, also known as the Position equations, represent the rate of change of the translational position. These equations are based on the transformation of the translational velocity from the reference frame F_b to the reference frame F_o using following equation:

$$\dot{\vec{r}}_{Go} = \boldsymbol{C}_{ob}\, \vec{v}_{Gb} \tag{2.55}$$

The scalar form is shown below [11, 41]:

$$\begin{aligned} \dot{x}_{Go} = {} & u_{Gb} \cos\theta \cos\psi + v_{Gb} \left(\sin\phi \sin\theta \cos\psi - \cos\phi \sin\psi\right) \\ & + w_{Gb} \left(\cos\phi \sin\theta \cos\psi + \sin\phi \sin\psi\right) \end{aligned} \tag{2.56a}$$
$$\begin{aligned} \dot{y}_{Go} = {} & u_{Gb} \cos\theta \sin\psi + v_{Gb} \left(\sin\phi \sin\theta \sin\psi + \cos\phi \cos\psi\right) \\ & + w_{Gb} \left(\cos\phi \sin\theta \sin\psi - \sin\phi \cos\psi\right) \end{aligned} \tag{2.56b}$$
$$\dot{z}_{Go} = -u_{Gb} \sin\theta + v_{Gb} \sin\phi \cos\theta + w_{Gb} \cos\phi \cos\theta \tag{2.56c}$$

The rate of change of the translational position, based on Equation 2.3, can also be expressed in the Geodetic coordinate system as:

$$\dot{\ell} = \frac{\dot{y}_{Go}}{\left(N_0 + h\right) \cos\varphi} \tag{2.57a}$$
$$\dot{\varphi} = \frac{\dot{x}_{Go}}{M_0 + h} \tag{2.57b}$$
$$\dot{h} = -\dot{z}_{Go} \tag{2.57c}$$

The **Velocity equations** describe the rate of change of the translational velocity. The Velocity equation is based on Equation 2.23 for the Translational acceleration in rotating reference frames. Given that the total acceleration can be decomposed into specific force and gravitational acceleration (see Equation 2.30), and that the acceleration is the first derivative of the velocity, the resulting equation can be written as

$$\dot{\vec{v}}_{Gb} = \vec{f}_G + \vec{g}_0 - \vec{\omega}_{ob} \times \vec{v}_{Gb} \tag{2.58}$$

Based on the Equations 2.31, Equation 2.58 can be given in the scalar form:

$$\dot{u}_{Gb} = f_x - G_0 \sin\theta + r\, v_{Gb} - q\, w_{Gb} \tag{2.59a}$$
$$\dot{v}_{Gb} = f_y + G_0 \cos\theta \sin\phi + p\, w_{Gb} - r\, u_{Gb} \tag{2.59b}$$
$$\dot{w}_{Gb} = f_z + G_0 \cos\theta \cos\phi + q\, u_{Gb} - p\, v_{Gb} \tag{2.59c}$$

2.4.3 Nonlinear dynamic Equations of Motion

Nonlinear dynamic EoM describe the forces and moments acting on the airplane. As it was mentioned before, there are three sources of forces and moments acting on an airplane in flight: the aerodynamic forces and moments, the propulsion forces and moments and finally the gravitational force. Gravitation does not generate moment, as the gravitational force is acting in the center of mass. Particular models of these forces and moments were introduced in Section 2.3.

Force equations describes the rate of change of the translational velocity. The Force equations are based on the Velocity equation given in 2.58, which is extended using substitution of the specific force with Equation 2.30 to include the forces affecting the motion of the airplane. The resultant Force equation is:

$$\dot{\vec{v}}_{Gb} = \frac{\vec{F}_A + \vec{F}_P + \vec{G}_G}{m} - \vec{\omega}_{ob} \times \vec{v}_{Gb} \tag{2.60}$$

Based on the Equations 2.31, 2.49 and 2.43, the Force equation can be expressed in the scalar form:

$$\dot{u}_{Gb} = \frac{\bar{q}S}{m} C_X + \frac{F_P}{m} - G_0 \sin\theta + r\, v_{Gb} - q\, w_{Gb} \tag{2.61a}$$
$$\dot{v}_{Gb} = \frac{\bar{q}S}{m} C_Y + G_0 \cos\theta \sin\phi + p\, w_{Gb} - r\, u_{Gb} \tag{2.61b}$$
$$\dot{w}_{Gb} = \frac{\bar{q}S}{m} C_Z + G_0 \cos\theta \cos\phi + q\, u_{Gb} - p\, v_{Gb} \tag{2.61c}$$

The Force equations can be also expressed in the Spherical coordinate system utilizing Equations 2.7, 2.9, 2.31, 2.49 and 2.43. The resultant equations are:

$$\begin{aligned}\dot{V} = & -\frac{\bar{q}S}{m} C_W + \frac{F_P}{m} \cos\beta\, \cos\alpha \\ & + G_0 (\sin\beta \cos\theta \sin\phi + \cos\beta \sin\alpha \cos\theta \cos\phi - \cos\beta \cos\alpha \sin\theta)\end{aligned} \tag{2.62a}$$
$$\begin{aligned}\dot{\alpha} = & -\frac{\bar{q}S}{m\,V\, \cos\beta} C_L - \frac{F_P\, \sin\alpha}{m\,V\, \cos\beta} - p\, \cos\alpha\, \tan\beta + q - r\, \sin\alpha\, \tan\beta \\ & + \frac{G_0}{V\, \cos\beta} (\cos\alpha\, \cos\theta \cos\phi + \sin\alpha\, \sin\theta)\end{aligned} \tag{2.62b}$$
$$\dot{\beta} = \frac{\bar{q}S}{m\,V} C_Q - \frac{F_P}{m\,V} \sin\beta\, \cos\alpha + p\, \sin\alpha - r\, \cos\alpha$$

$$+\frac{G_0}{V}\left[\cos\beta\cos\theta\sin\phi+\sin\beta\left(\cos\alpha\sin\theta-\sin\alpha\cos\theta\cos\phi\right)\right] \tag{2.62c}$$

Moment equations represents the rate of change of the angular velocity. Moment equations are based on Equation 2.39 for the Moment of forces in rotating reference frames. Given that the moment of force acting on an airplane can be decomposed into a moment of aerodynamic force and a moment of propulsion force, the resultant equation is

$$\boldsymbol{J}_b\,\vec{\alpha}_{ob}=\vec{\tau}_A+\vec{\tau}_P-\vec{\omega}_{ob}\times\boldsymbol{J}_b\,\vec{\omega}_{ob} \tag{2.63}$$

This equation can be written in scalar form using Equations 2.33, 2.51 and 2.45 as follows [25]:

$$\begin{aligned}\dot{p}\,J_x-\dot{q}\,J_{xy}-\dot{r}\,J_{xz}&=\bar{q}\,S\,b_w\,C_l-J_P\,\dot{\omega}_P+\\&\qquad q\,r\left(J_y-J_z\right)+J_{yz}\left(q^2-r^2\right)+p\,q\,J_{xz}-p\,r\,J_{xy}\end{aligned} \tag{2.64a}$$

$$\begin{aligned}-\dot{p}\,J_{xy}+\dot{q}\,J_y-\dot{r}\,J_{yz}&=\bar{q}\,S\,\bar{c}\,C_m+J_P\,r\,\omega_P+F_P\,z_P+\\&\qquad p\,r\left(J_z-J_x\right)+J_{xz}\left(r^2-p^2\right)+q\,r\,J_{xy}-p\,q\,J_{yz}\end{aligned} \tag{2.64b}$$

$$\begin{aligned}-\dot{p}\,J_{xz}-\dot{q}\,J_{yz}+\dot{r}\,J_z&=\bar{q}\,S\,b_w\,C_n-J_P\,q\,\omega_P-F_P\,y_P+\\&\qquad p\,q\left(J_x-J_y\right)+J_{xy}\left(p^2-q^2\right)+p\,r\,J_{yz}-q\,r\,J_{xz}\end{aligned} \tag{2.64c}$$

Given that airplane's plane of symmetry is x_bz_b and center of mass of aircraft is lying on this plane, inertia elements J_{xy} and J_{yz} are equal to zero (see Equation 2.35). Therefore Equation 2.64 can be simplified to

$$\dot{p}\,J_x-\dot{r}\,J_{xz}=\bar{q}\,S\,b_w\,C_l-J_P\,\dot{\omega}_P+q\,r\left(J_y-J_z\right)+p\,q\,J_{xz} \tag{2.65a}$$

$$\dot{q}\,J_y=\bar{q}\,S\,\bar{c}\,C_m+J_P\,r\,\omega_P+F_P\,z_P+p\,r\left(J_z-J_x\right)+J_{xz}\left(r^2-p^2\right) \tag{2.65b}$$

$$-\dot{p}\,J_{xz}+\dot{r}\,J_z=\bar{q}\,S\,b_w\,C_n-J_P\,q\,\omega_P-F_P\,y_P+p\,q\left(J_x-J_y\right)-q\,r\,J_{xz} \tag{2.65c}$$

and solved for $\dot{p}$, $\dot{q}$, and $\dot{r}$ as follows

$$\begin{aligned}\dot{p}=&\frac{\bar{q}\,S\,b_w\left(J_z\,C_l+J_{xz}\,C_n\right)-J_{xz}\left(J_P\,q\,\omega_P+F_P\,Pb\right)-J_z\,J_P\,\dot{\omega_P}}{J_x\,J_z-J_{xz}^2}+\\&\frac{p\,q\,J_{xz}\left(J_x-J_y+J_z\right)+q\,r\,\left(J_y\,J_z-J_z^2-J_{xz}^2\right)}{J_x\,J_z-J_{xz}^2}\end{aligned} \tag{2.66a}$$

$$\dot{q}=\frac{\bar{q}\,S\bar{c}\,C_m-J_P\,r\,\omega_P+F_{Pb}\,z_{Pb}+p\,r\left(J_z-J_x\right)+J_{xz}\left(r^2-p^2\right)}{J_y} \tag{2.66b}$$

$$\begin{aligned}\dot{r}=&\frac{\bar{q}\,S\,b_w\left(J_{xz}\,C_l+J_x\,C_n\right)-J_x\left(J_P\,q\,\omega_P+F_P\,y_{Pb}\right)-J_{xz}\,J_P\,\dot{\omega_P}}{J_x\,J_z-J_{xz}^2}+\\&\frac{p\,q\left(J_x^2-J_x\,J_y+J_{xz}^2\right)+q\,r\,J_{xz}\left(J_y-J_x-J_z\right)}{J_x\,J_z-J_{xz}^2}\end{aligned} \tag{2.66c}$$

2.4.4 Separation of dynamic Equations of Motion

There were four sets of the Equations of Motion presented before: Attitude equations, Navigation equation, Force equations (created from Velocity equations), and Moment equations.

The Navigation equations are used for the purposes of the Flight Path Reconstruction only; therefore, it is not necessary to linearize them.

The remaining three sets of the Equations of Motion contain nine equations, which can be separated according to the type of the motion to the Symmetric equations (motion in the vertical plane), i.e., V, α, q, and θ; and Antisymmetric equations (motion out of the vertical plane), i.e., β, p, r, and ϕ. In order to complete the division of the equations into these two categories, it is necessary to neglect dependencies of symmetric equations on antisymmetric variables and vice versa. The remaining, ninth, variable ψ could be theoretically included among Antisymmetric equations; however, it is often omitted, because ψ influences only the orientation of the airplane and does not influence the motion of the airplane (other antisymmetric variables are ψ-independent).

Symmetric equation for the longitudinal motion, i.e., equations of V, α, q, and θ, are created from Equations 2.62a, 2.62b, 2.66b, 2.54b, respectively. At first, the antisymmetric variables β, ϕ, p, and r are neglected, i.e., set equal to zero, to complete the separation of Symmetric and Antisymmetric equations. Then it is possible to substitute $\bar{q}$ with Equation 2.44. The resultant Symmetric equations are:

$$\dot{V} = -\frac{\rho\, V^2\, S}{2\, m}\, C_W + \frac{F_P}{m} \cos\alpha - G_0 \sin(\theta - \alpha) \tag{2.67a}$$

$$\dot{\alpha} = -\frac{\rho\, V\, S}{2\, m}\, C_L - \frac{F_P}{m\, V} \sin\alpha + q + \frac{G_0}{V} \cos(\theta - \alpha) \tag{2.67b}$$

$$\dot{q} = \frac{\rho\, V^2\, S\bar{c}}{2\, J_y}\, C_m + \frac{F_P\, z_{Pb}}{J_y} \tag{2.67c}$$

$$\dot{\theta} = q \tag{2.67d}$$

Antisymmetric equation for the lateral–directional motion, i.e., equations of β, p, r, and ϕ, are created from Equations 2.62c, 2.66a, 2.66c, 2.54a, respectively. The symmetric variables V, α, q, and θ are neglected, i.e., set equal to zero, to complete the separation of Symmetric and Antisymmetric equations. The resultant Symmetric equations are:

$$\dot{\beta} = \frac{\bar{q}\, S}{m\, V} C_Q + \frac{F_P}{m\, V} \sin\beta\, \cos\alpha + \frac{G_0\, \cos\alpha}{V} \big(\cos\beta \sin\phi - \sin\alpha \sin\beta\, (\cos\phi - 1)\big) + \\ p\, \sin\alpha - r\, \cos\alpha \tag{2.68a}$$

$$\dot{p} = \frac{\bar{q}\, S\, b_w\, (J_z\, C_l + J_{xz}\, C_n) - J_{xz}\, (J_P\, q\, \omega_P + F_P\, Pb) - J_z\, J_P\, \dot{\omega_P}}{J_x\, J_z - J_{xz}^2} \tag{2.68b}$$

$$\dot{r} = \frac{\bar{q}\, S\, b_w\, (J_{xz}\, C_l + J_x\, C_n) - J_x\, (J_P\, q\, \omega_P + F_P\, y_{Pb}) - J_{xz}\, J_P\, \dot{\omega_P}}{J_x\, J_z - J_{xz}^2} \tag{2.68c}$$

$$\dot{\phi} = p + r \frac{\tan\alpha}{\cos\phi} \tag{2.68d}$$

2.5 Linear Equations of Motion

In this section, system linearization including definition of the linear state–space model and derivation of a linearized system is described. At the end, the linearized Equations of Motion are given.

2.5.1 System linearization

Dynamic systems can be divided into two separate categories: nonlinear systems and linear systems. The difference between them is, that linear systems have to satisfy the property of superposition, which is defined by the following equations [3, 8]:

$$f(u_1 + u_2) = f(u_1) + f(u_2) \quad \wedge \quad f(k\,u_1) = k\,f(u_1) \tag{2.69}$$

where k is an arbitrary scalar.

There are many approaches to describe linear systems. In aviation, state–space model is the most commonly used one. The state–space model of a linear system is given by the equations [5, 8]:

$$\dot{\vec{x}} = \boldsymbol{A}\vec{x} + \boldsymbol{B}\vec{u} \tag{2.70a}$$

$$\vec{y} = \boldsymbol{C}\vec{x} + \boldsymbol{D}\vec{u} \tag{2.70b}$$

$$\vec{x}(0) = \vec{x}_0 \tag{2.70c}$$

where $\boldsymbol{A}$ is the state/system matrix, $\boldsymbol{B}$ is the input matrix, $\boldsymbol{C}$ is the output matrix, $\boldsymbol{D}$ is the feed-through/feed-forward matrix.

The nonlinear system described by the dynamic equations can be transformed into a linear system described by a state–space model using the following linearization process. Lets assume, that the deflections $\Delta\,\vec{x}$ and $\Delta\,\vec{u}$ from a trim/equilibrium point (x_t, u_t) and are very small [40, 41] and can be computed as follows:

$$\Delta\,\vec{x} = \vec{x} - \vec{x}_t \tag{2.71a}$$

$$\Delta\,\vec{u} = \vec{u} - \vec{u}_t \tag{2.71b}$$

and the first derivative of $\vec{x}_t$, i.e., result of the state function in the trim/equilibrium point is:

$$\dot{\vec{x}}_t = f(\vec{x}_t, \vec{u}_t) = 0 \tag{2.72}$$

Then Equation 2.53a can be modified to:

$$\dot{\vec{x}}_t + \Delta\dot{\vec{x}} = f(\vec{x}_t + \Delta\vec{x}, \vec{u}_t + \Delta\vec{u}) \tag{2.73}$$

This equation can be further expanded using Taylor series and neglecting the high-order terms [40, 41]. The resultant equation is:

$$\dot{\vec{x}}_t + \Delta\dot{\vec{x}} = f(\vec{x}_t, \vec{u}_t) + \frac{\partial f}{\partial \vec{x}}\Delta\vec{x} + \frac{\partial f}{\partial \vec{u}}\Delta\vec{u} \tag{2.74}$$

where $\frac{\partial f}{\partial \vec{x}}$ and $\frac{\partial f}{\partial \vec{u}}$ are the Jacobian matrices constructed as:

$$\frac{\partial f}{\partial \vec{x}} = \begin{bmatrix} \frac{\partial f_1}{\partial x_1} & \frac{\partial f_1}{\partial x_2} & \cdots & \frac{\partial f_1}{\partial x_{n_x}} \\ \frac{\partial f_2}{\partial x_1} & \frac{\partial f_2}{\partial x_2} & \cdots & \frac{\partial f_1}{\partial x_{n_x}} \\ \vdots & \vdots & \ddots & \vdots \\ \frac{\partial f_{n_x}}{\partial x_1} & \frac{\partial f_{n_x}}{\partial x_2} & \cdots & \frac{\partial f_{n_x}}{\partial x_{n_x}} \end{bmatrix} \tag{2.75}$$

$$\frac{\partial f}{\partial \vec{u}} = \begin{bmatrix} \frac{\partial f_1}{\partial u_1} & \frac{\partial f_1}{\partial u_2} & \cdots & \frac{\partial f_1}{\partial u_{nu}} \\ \frac{\partial f_2}{\partial u_1} & \frac{\partial f_2}{\partial u_2} & \cdots & \frac{\partial f_1}{\partial u_{nu}} \\ \vdots & \vdots & \ddots & \vdots \\ \frac{\partial f_{nx}}{\partial u_1} & \frac{\partial f_{nx}}{\partial u_2} & \cdots & \frac{\partial f_{nx}}{\partial u_{nu}} \end{bmatrix} \tag{2.76}$$

The Jacobian matrices $\frac{\partial f}{\partial \vec{x}}$ and $\frac{\partial f}{\partial \vec{u}}$ are equal to the state/system matrix $\boldsymbol{A}$ and the input matrix $\boldsymbol{B}$ of the state–space model, respectively.

The Output equation of the dynamic model (Equation 2.53b) can be processed using the same, above-mentioned approach. The resultant matrices will have following form:

$$\boldsymbol{C} = \frac{\partial h}{\partial \vec{x}} \tag{2.77a}$$

$$\boldsymbol{D} = \frac{\partial h}{\partial \vec{u}} \tag{2.77b}$$

2.5.2 Linear Equations of Motion

The process described in Section 2.5.1 can be used to linearize nonlinear Equations of Motion introduced in Section 2.4. These resultant equations can be separated into sets of Symmetric and Antisymmetric equations.

Symmetric equations for the longitudinal motion, after the linearization procedure are described by the resultant state–space model shown below:

$$\begin{bmatrix} \dot{V} \\ \dot{\alpha} \\ \dot{q} \\ \dot{\theta} \end{bmatrix} = \begin{bmatrix} D_V & D_\alpha & D_q & D_\theta \\ L_V & L_\alpha & L_q & L_\theta \\ M_V & M_\alpha & M_q & 0 \\ 0 & 0 & 1 & 0 \end{bmatrix} \begin{bmatrix} V \\ \alpha \\ q \\ \theta \end{bmatrix} + \begin{bmatrix} D_{\delta_e} & D_{F_P} \\ L_{\delta_e} & L_{F_P} \\ M_{\delta_e} & M_{F_P} \\ 0 & 0 \end{bmatrix} \begin{bmatrix} \delta_e \\ F_P \end{bmatrix} \tag{2.78}$$

where particular elements of respective matrices can be expressed as:

$$D_V = -\frac{\rho\, V\, S}{m}\left(C_{W0} + \alpha\, C_{W\alpha} + \delta_e\, C_{W\delta_e} + \frac{\bar{c}\, q}{4\, V} C_{Wq}\right) \tag{2.79a}$$

$$D_\alpha = -\frac{\rho\, V^2\, S}{2\, m} C_{W\alpha} - \frac{F_P}{m} \sin\alpha + G_0 \cos(\theta - \alpha) \tag{2.79b}$$

$$D_q = -\frac{\rho\, V\, S\, \bar{c}}{4\, m} C_{Wq} \tag{2.79c}$$

$$D_\theta = -G_0 \cos(\theta - \alpha) \tag{2.79d}$$

$$D_{\delta_e} = -\frac{\rho\, V^2\, S}{2\, m} C_{W\delta_e} \tag{2.79e}$$

$$D_{F_P} = \frac{\cos\alpha}{m} \tag{2.79f}$$

$$L_V = \frac{F_P \sin\alpha}{V^2\, m} - \frac{\rho\, S}{2\, m}\left(C_{L0} + \alpha\, C_{L\alpha} + \delta_e\, C_{L\delta_e} + \frac{\bar{c}\, q\, C_{Lq}}{V}\right) - \frac{G_0}{V^2} \cos(\theta - \alpha) \tag{2.79g}$$

$$L_\alpha = \frac{G_0}{V} \sin(\theta - \alpha) - \frac{\rho\, V\, S}{2\, m} C_{L\alpha} + \frac{F_P \cos\alpha}{V\, m} \tag{2.79h}$$

$$L_q = 1 - \frac{\rho\, S\, \bar{c}}{4\, m} C_{Lq} \tag{2.79i}$$

$$L_\theta = -\frac{G_0}{V}\,\sin\left(\theta - \alpha\right) \tag{2.79j}$$

$$L_{\delta_e} = -\frac{\rho\, V\, S}{2\, m} C_{L\delta_e} \tag{2.79k}$$

$$L_{F_P} = -\frac{\sin\alpha}{V\, m} \tag{2.79l}$$

$$M_V = \frac{\rho\, V\, S\, \bar{c}}{J_y}\left(C_{m0} + \alpha\, C_{m\alpha} + \delta_e\, C_{m\delta_e} + \frac{\bar{c}\, q}{4\, V} C_{mq}\right) \tag{2.79m}$$

$$M_\alpha = \frac{\rho\, V^2\, S\, \bar{c}}{2\, J_y} C_{m\alpha} \tag{2.79n}$$

$$M_q = \frac{\rho\, V\, S\, \bar{c}^{\,2}}{4\, J_y} C_{mq} \tag{2.79o}$$

$$M_{\delta_e} = \frac{\rho\, V^2\, S\, \bar{c}}{2\, J_y} C_{m\delta_e} \tag{2.79p}$$

$$M_{F_P} = \frac{z_P}{J_y} \tag{2.79q}$$

3. Flight parameter estimation

Parameter estimation consists of following elements: optimization algorithm, identification criteria, mathematical model, model structure and model requirements. The process of parameter estimation has following prerequisites: Flight Path Reconstruction and a–priori values. The result of parameter estimation process is subjected to the model validation. For the description of the whole process flow, see Figure 3.1.

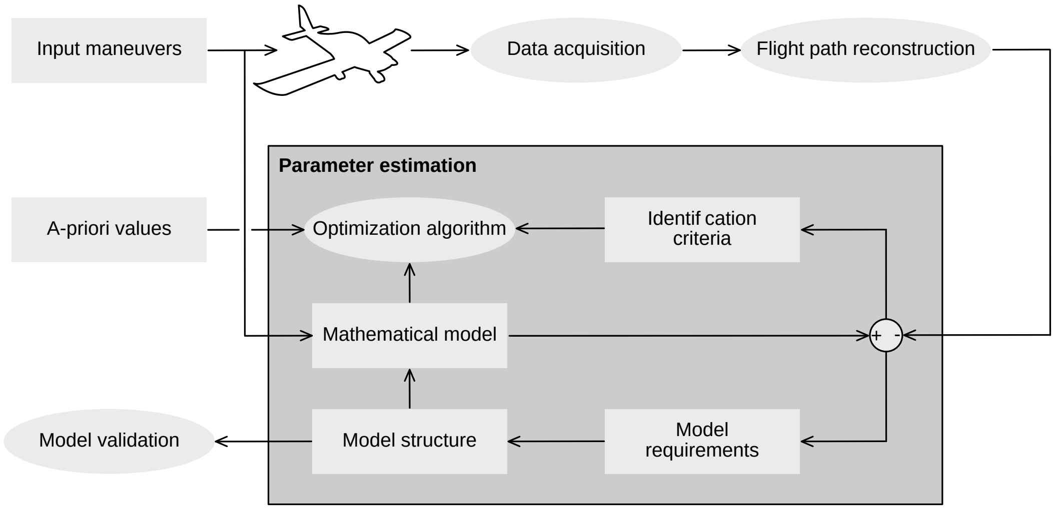

Figure 3.1: Identification process flow.

The Section 3.1 discuses sensor errors and the Flight Path Reconstruction process. The description of the sources of a–priori values of respective aerodynamic parameters is given in Section 3.2. The estimation methods for the estimation of the flight parameters of a light airplane are discussed in Section 3.3.

3.1 Flight Path Reconstruction

All sensor outputs are affected by errors. The output of the sensors is effected by the deterministic and stochastic errors. Deterministic errors contain the sensor errors and the position errors. Stochastic errors are difficult to predict, e.g., noise. Hence, some of the variables are measured by more than one sensor, or estimated using the integration or derivation of specific variable. It is also possible to use a redundancy in sensor output as a way to minimize some of the errors.

Some sensors do not directly measure required quantity, but the required quantity can be estimated from these measurements. The angle–of–sideslip cannot be measured directly, but it is convenient to measure the flank angle. Measured flank angle β_f is further used for the computation of the angle–of–sideslip using Equation [25, 30]:

$$\beta = \arctan\left(\tan \beta_f \cdot \cos \alpha\right) \tag{3.1}$$

First part of this section introduces common sensor errors. In the following part, the position errors of the sensors are described. Further, the measurement and the process noises are analyzed. At the end of this section, Kalman Filter and its variants are discussed.

3.1.1 Bias and gain error

Most of the sensor outputs contain sensor errors, and most sensors errors can be corrected by calibration.

The direction of the airflow sensors suffers from sensors errors which can be compensated using gains and bias values. The sensor error in the direction of the airflow sensor is caused by the pressure field created around the airplane. The effect on the flow vanes is also called upwash or sidewash and can be computed using the equation:

$$\alpha_m = K_\alpha \, \alpha + b_\alpha \tag{3.2a}$$

$$\beta_{fm} = K_\beta \, \beta_f + b_{\beta_f} \tag{3.2b}$$

where α_m is the measured angle–of–attack, β_{fm} is the measured flank angle, b_α and b_β are the biases, and K_α and K_β are the scale factors caused by upwash or sidewash.

3.1.2 Position error

The position error affects the sensor output due to an inconvenient installation position of the sensor or an incorrect axis alignment.

An accelerometer output suffers from an incorrect installation position relative to the airplane centre of mass, as the center of mass is changing during the flight as a result of the fuel consumption as introduced in Section 2.3.1. Given that the specific force is a type of acceleration, the specific force of the whole airplane can be computed using an acceleration Equation 2.24. The resultant equation can be simplified by neglecting the velocity of change of accelerometers position to [22, 47]:

$$\vec{f}_G = \vec{f}_C + \begin{bmatrix} \left(q^2 + r^2\right) & -\left(p\,q - \dot{r}\right) & -\left(p\,r + \dot{q}\right) \\ -\left(p\,q + \dot{r}\right) & \left(p^2 + r^2\right) & -\left(q\,r - \dot{p}\right) \\ -\left(p\,r - \dot{q}\right) & -\left(q\,r + \dot{p}\right) & \left(p^2 + q^2\right) \end{bmatrix} \cdot \vec{r}_C \tag{3.3}$$

where $\vec{f}_C$ is the specific force measured by the accelerometer, which is installed in position $\vec{r}_C$ in the reference frame F_b.

In addition to that the position of the direction of the airflow sensors cause an apparent velocity due to airplane rotation. Equation 2.22 describes this effect in following form:

$$u_{Xb} = u_{Gb} + q_{ob}\, z_{Xb} - r_{ob}\, y_{Xb} \tag{3.4a}$$

$$v_{Xb} = v_{Gb} + r_{ob}\, x_{Xb} - p_{ob}\, z_{Xb} \tag{3.4b}$$

$$w_{Xb} = w_{Gb} + p_{ob}\, y_{Xb} - q_{ob}\, x_{Xb} \tag{3.4c}$$

3.1.3 Measurement and process noise

The measurement noise describes the stochastic error of a sensor. The measurement noise of most of the sensors exhibits Gaussian normal distribution.

The probability density function $p(\vec{\chi})$ of a normal distribution $\mathbb{N}$ of a general $\vec{\chi} \sim \mathbb{N}\left(\vec{\mu}_\chi, \mathbf{\Sigma}_\chi\right)$ is defined as:

$$p(\vec{\chi}) = \frac{1}{\sqrt{(2\pi)^{n_\chi} \det\left(\mathbf{\Sigma}_\chi\right)}} \exp\left(-\frac{1}{2}\left(\vec{\chi} - \vec{\mu}_\chi\right)^T \mathbf{\Sigma}_\chi^{-1}\left(\vec{\chi} - \vec{\mu}_\chi\right)\right) \tag{3.5}$$

where n_χ is the count of elements of $\vec{\chi}$, $\mathbf{\Sigma}$ is a covariance matrix of normal distribution and $\vec{\mu}$ is a mean of normal distribution.

The process noise is the way to resolve uncertainties in inputs to a dynamic system.

Because input variables are measured similarly to output variables, process noise has also a normal distribution. For the purposes of this thesis, the turbulence is neglected.

3.1.4 Kalman Filter

Kalman Filter is based on the nonlinear kinematic Equations of motion described in Section 2.4.2.

A bayesian model for the uncertainties is based on the Bayesian estimation theory and assumed a–priori known probability densities of $p\left(\vec{\theta}\right)$ and $p(\vec{\nu})$. The conditional probability density $p\left(\vec{\theta}\middle|\vec{z}\right)$ can be expressed using the Bayes' rule as:

$$p\left(\vec{\theta}\middle|\vec{z}\right) = \frac{p\left(\vec{z}\middle|\vec{\theta}\right) p\left(\vec{\theta}\right)}{p(\vec{z})} \tag{3.6}$$

where $\vec{\theta}$ is the vector of parameters and $\vec{z}$ is the measured output vector.

If $\vec{\theta}$ has a normal distribution defined as:

$$\vec{\theta} \quad \sim \quad \mathbb{N}\left(\vec{\theta}_p, \mathbf{\Sigma}_p\right) \tag{3.7}$$

then $p\left(\vec{\theta}\right)$ is:

$$p\left(\vec{\theta}\right) = \frac{1}{\sqrt{(2\pi)^n \det\left(\mathbf{\Sigma}_p\right)}} \exp\left(-\frac{1}{2}\left(\vec{\theta} - \vec{\theta}_p\right)^T \mathbf{\Sigma}_p^{-1}\left(\vec{\theta} - \vec{\theta}_p\right)\right) \tag{3.8}$$

where n is the number of parameters.

The probability density $p\left(\vec{\theta}\middle|\vec{z}\right)$ can be expressed using Equation 3.6 as:

$$p\left(\vec{\theta}\middle|\vec{z}\right) = \frac{1}{p(\vec{z})} \frac{1}{\sqrt{(2\pi)^{N+n} \det(\boldsymbol{R}) \det\left(\mathbf{\Sigma}_p\right)}}$$

$$\exp\left(-\frac{1}{2}\left(\vec{z}-\boldsymbol{X}\vec{\theta}\right)^T \boldsymbol{R}^{-1}\left(\vec{z}-\boldsymbol{X}\vec{\theta}\right)-\frac{1}{2}\left(\vec{\theta}-\vec{\theta}_p\right)^T \boldsymbol{\Sigma}_p^{-1}\left(\vec{\theta}-\vec{\theta}_p\right)\right) \tag{3.9}$$

where $\boldsymbol{R}$ is the measurement noise covariance matrix, $\boldsymbol{X}$ is the matrix of regressors and with the most probable estimate $\hat{\vec{\theta}}$ being:

$$\hat{\vec{\theta}} = \max_{\vec{\theta}} p\left(\vec{\theta}\middle|\vec{z}\right) \tag{3.10}$$

The cost function $J\left(\right)$ for minimization is derived to have following form:

$$J\left(\vec{\theta}\right) = \frac{1}{2}\left(\vec{z}-\boldsymbol{X}\vec{\theta}\right)^T \boldsymbol{R}^{-1}\left(\vec{z}-\boldsymbol{X}\vec{\theta}\right)+\frac{1}{2}\left(\vec{\theta}-\vec{\theta}_p\right)^T \boldsymbol{\Sigma}_p^{-1}\left(\vec{\theta}-\vec{\theta}_p\right) \tag{3.11}$$

A discrete state–space model can be described by following set of equations:

$$\vec{x}\left(k+1\right) = \boldsymbol{\Phi}\vec{x}\left(k\right)+\boldsymbol{\Gamma}\vec{u}\left(k\right) \tag{3.12a}$$
$$\vec{y}\left(k\right) = \boldsymbol{C}\vec{x}\left(k\right)+\boldsymbol{D}\vec{u}\left(k\right) \tag{3.12b}$$
$$\vec{x}\left(0\right) = \vec{x}_0 \tag{3.12c}$$

where k is the sample number, $\boldsymbol{\Phi}$ is the discrete state matrix and $\boldsymbol{\Gamma}$ is the discrete input matrix.

The transformation of the continuous state–space matrices to the discrete state–space matrices becames [5, 14]:

$$\boldsymbol{\Phi} = e^{\boldsymbol{A}\delta t} \quad\Rightarrow\quad \boldsymbol{\Phi} = \boldsymbol{I}+\boldsymbol{A}\delta t+\boldsymbol{A}^2\frac{\delta t^2}{2!}+\boldsymbol{A}^3\frac{\delta t^3}{3!}+\cdots \tag{3.13}$$

$$\boldsymbol{\Gamma} = \int_0^{\delta t} e^{\boldsymbol{A}\delta t}\boldsymbol{B} \quad\Rightarrow\quad \boldsymbol{\Gamma} = \boldsymbol{B}\delta t+\boldsymbol{A}\frac{\delta t^2}{2!}\boldsymbol{B}+\boldsymbol{A}^2\frac{\delta t^3}{3!}\boldsymbol{B}+\cdots \tag{3.14}$$

where δt is a time step.

The most commonly used state estimation algorithm is the Kalman Filter (KF). The KF algorithm is divided into the prediction step and the correction step. The prediction step uses the system input to predict the probable state. Correction step uses a noisy measurement to improve the prediction of the state. The basic KF is a discrete version of the **Linear Kalman Filter**. The Linear Kalman Filter is an optimal estimator [27].

Assuming a discrete linear dynamic system with a process and measurement noises and a zero feed–through matrix as described by equation [27]:

$$\vec{x}\left(k+1\right) = \boldsymbol{\Phi}\,\vec{x}\left(k\right)+\boldsymbol{\Gamma}\,\vec{u}\left(k\right)+\boldsymbol{\Lambda}\,\vec{w}\left(k\right) \tag{3.15a}$$
$$\vec{z}\left(k\right) = \boldsymbol{C}\,\vec{x}\left(k\right)+\vec{\nu}\left(k\right) \tag{3.15b}$$
$$\vec{x}\left(0\right) = \vec{x}_0 \tag{3.15c}$$

where $\boldsymbol{\Lambda}$ is a discrete noise input matrix and $\vec{w}$ is the process noise with a normal distribution defined as:

$$\vec{w} \quad\sim\quad \mathbb{N}\left(0,\boldsymbol{Q}\right) \tag{3.16}$$

where $\boldsymbol{Q}$ is the process noise covariance matrix.

The prediction step of a Linear Kalman Filter is defined using following equation:

$$\vec{x}\,(k+1|k) = \mathbf{\Phi}\,\vec{x}\,(k|k) + \mathbf{\Gamma}\,\vec{u}\,(k) \tag{3.17}$$

where $\vec{x}\,(k+1|k)$ is the state vector in step $k+1$ based on information in step k.

The prediction of the probability of state $\vec{x}$ is $\boldsymbol{P}$ defined in equation:

$$\boldsymbol{P}\,(k+1|k) = \mathbf{\Phi}\,\boldsymbol{P}\,(k|k)\,\mathbf{\Phi}^T + \mathbf{\Lambda}\,\boldsymbol{Q}\,\mathbf{\Lambda}^T \tag{3.18}$$

The correction step of a Linear Kalman Filter is defined using following equation:

$$\vec{x}\,(k+1|k+1) = \vec{x}\,(k+1|k) + \boldsymbol{K}_{k+1}\left[\vec{z}\,(k+1) - \boldsymbol{C}\,\vec{x}\,(k+1|k)\right] \tag{3.19}$$

where $\boldsymbol{K}_{k+1}$ is the Kalman gain matrix in step $k+1$ defined in equation:

$$\boldsymbol{K}_{k+1} = \boldsymbol{P}\,(k+1|k)\,\boldsymbol{C}^T\left[\boldsymbol{C}\,\boldsymbol{P}\,(k+1|k)\,\boldsymbol{C}^T + \boldsymbol{R}\right]^{-1} \tag{3.20}$$

The correction of the probability of state $\vec{x}$ is $\boldsymbol{P}$ defined in following equation:

$$\boldsymbol{P}\,(k+1|k+1) = \left[\boldsymbol{I} - \boldsymbol{K}_{k+1}\boldsymbol{C}\right]\boldsymbol{P}\,(k+1|k) \tag{3.21}$$

The **Extended Kalman Filter** (EKF) is an approximate filter for nonlinear systems, based on local first-order linearization (see Section 2.5.1) and utilization of Linear Kalman Filter.

Assume discrete continuous dynamic system without feed–through inputs described by equation:

$$\vec{x}\,(k+1) = f'\left(\vec{x}\,(k),\vec{u}\,(k),\vec{w}\,(k)\right) \tag{3.22a}$$
$$\vec{y}\,(k) = h'\left(\vec{x}\,(k)\right) + \vec{\nu}\,(k) \tag{3.22b}$$
$$\vec{x}\,(0) = \vec{x}_0 \tag{3.22c}$$

where $f'\,()$ is the discrete state function and $h'\,()$ is the discrete output function.

The prediction step of the Extended Kalman Filter is defined using the equation:

$$\vec{x}\,(k+1|k) = f'\left(\vec{x}\,(k|k),\vec{u}\,(k),0\right) \tag{3.23}$$

Prediction of the probability of the state $\vec{x}$ is $\boldsymbol{P}$ defined in Equation 3.18 in which $\mathbf{\Phi}$ and $\mathbf{\Lambda}$ are equal to:

$$\mathbf{\Phi} = \frac{\partial f'\left(\vec{x}\,(k|k),\vec{u}\,(k),0\right)}{\partial\vec{x}} \tag{3.24a}$$
$$\mathbf{\Lambda} = \frac{\partial f'\left(\vec{x}\,(k|k),\vec{u}\,(k),0\right)}{\partial\vec{w}} \tag{3.24b}$$

The correction step of a Extended Kalman Filter is defined using equation:

$$\vec{x}\,(k+1|k+1) = \vec{x}\,(k+1|k) + \boldsymbol{K}_{k+1}\left[\vec{z}\,(k+1) - h'\left(\vec{x}\,(k+1|k)\right)\right] \tag{3.25}$$

where $\boldsymbol{K}_{k+1}$ is the Kalman gain matrix, computed using Equation 3.20 and $\boldsymbol{C}$ is the defined in equation:

$$\boldsymbol{C} = \frac{\partial h'\left(\vec{x}\left(k+1|k\right)\right)}{\partial \vec{x}} \tag{3.26}$$

The correction of probability of state $\vec{x}$ is $\boldsymbol{P}$ defined in Equation 3.21.

Because the EKF use local linearization, it is no longer an optimal estimator. **Iterative EKF** uses internal iteration to compensate inaccuracies from linearization of output equation [29, 47].

The prediction step uses EKF Equations 3.18, 3.23 and 3.24.

The correction step is iterative and it starts with assigning $\vec{\eta}_1$ to predicted state:

$$\vec{\eta}_1 = \vec{x}\left(k+1|k\right) \tag{3.27}$$

Next, output matrix $\boldsymbol{C}$ and Kalman gain $\boldsymbol{K}$ are computed using Equations 3.26 and 3.20. Then, new corrected state $\vec{\eta}_2$ is computed using equation:

$$\vec{\eta}_2 = \vec{x}\left(k+1|k\right) + \boldsymbol{K}_{k+1}\left[\vec{z}\left(k+1\right) - h'\left(\vec{\eta}_1\right) - \boldsymbol{C}\left(\vec{x}\left(k+1|k\right) - \vec{\eta}_1\right)\right] \tag{3.28}$$

Iteration stops if condition of inequality 3.29 is met:

$$\vec{\epsilon} \geq \frac{\|\vec{\eta}_2 - \vec{\eta}_1\|}{\|\vec{\eta}_1\|} \tag{3.29}$$

Next iteration starts with assigning $\vec{\eta}_1$ to last estimate $\vec{\eta}_2$:

$$\vec{\eta}_1 = \vec{\eta}_2 \tag{3.30}$$

After the stop of iteration process, the corrected state is equal to:

$$\vec{x}\left(k+1|k+1\right) = \vec{\eta}_2 \tag{3.31}$$

The correction of the probability of the state $\vec{x}$ is $\boldsymbol{P}$ defined in Equation 3.21.

3.2 A–priori values acquisition

A–priori aerodynamic parameters are usually computed using predictive tools, based on statistical data or advanced numerical simulations. Prediction tools based on the Vortex Lattice Method (VLM) theory, mainly software packages Tornado and Athena Vortex Lattice (AVL) were used in this thesis. To augment the computed results with a set of differently estimated data, the United States Air Force (USAF) Datcom predictions have been utilized.

All above mentioned sources of the a–priori values are described in detail in following sections.

3.2.1 Tornado

The Tornado is a VLM software for the estimation of flight parameters on the basis of airplane geometry [32]. The shape of the airplane is transformed to its planar representation featuring respective airfoil data. The planar representation of the airplane serves as an input for the solver.

A missing support for fuselage parts modeling is the main disadvantage of the Tornado calculations. Although the fuselage can be substituted by its planar representation or can be completely omitted for the case of longitudinal motion analysis.

The Tornado software covers the effects of the linear aerodynamics [32], which can limit its usability. However, for the purposes of this thesis its prediction fall into the region of validity.

The Tornado software is programmed in Matlab and distributed as source code under a GNU General Public License.

3.2.2 AVL

The AVL (Athena Vortex Lattice) is a VLM software for the analysis of a rigid aircraft flight mechanics [10]. For the output, the AVL offers linearization of the flight parameters in any flight state and mass properties settings. Linearization is based on small perturbations theory and is not completely valid when velocity perturbations from the free-stream become large.

The main advantage of AVL is the support of a slender–body models for fuselages and nacelles. All bodies has to have circular cross–section. According to manual, the non–round bodies must be approximated with an equivalent round body which has roughly the same cross–sectional areas.

The AVL software is programmed in Fortran and distributed in source code and binaries for major platforms. The AVL software is released under the GNU General Public License.

3.2.3 Datcom

The USAF Datcom is systematic summary of methods for estimating stability and control characteristics in preliminary design phase [49]. The Datcom was developed by McDonnell Douglas Corporation [49] under contract of USAF in cooperation with Wright–Patterson Air Force Base.

Limitations of Datcom is lack of support of the tapered wing, the H–tail and canard control surface. Those limitations are not important for light airplane category which is focus of this thesis.

The USAF Datcom is written completely in American National Standards Institute (ANSI) Fortran.

3.3 Estimation methods

Parameter estimation uses system models and optimization methods to estimate the values of investigated parameters.

The two basic approaches in estimation are the offline estimation and the online estimation. The offline estimation uses all measured values in all iterations of the algorithm. The online estimation uses currently measured values and previous estimate in current iteration of algorithm.

Two different estimators can be conveniently used for an offline parameter estimation: Least–Squares estimator and maximum likelihood estimator. Least–Squares is a simple estimator providing very good results. The maximum likelihood estimator requires complex knowledge of the investigated system, but its estimates provide high fidelity results.

There is a variety of estimation approaches for the estimation of the flight parameters. The most often used and also the most often recommended methods are: Equation Error Method (based on the Least–Squares estimator), Output Error Method (based on the maximum likelihood estimator) and Recursive Least–Squares (based on the Least–Squares estimator). These approaches are described in Sections 3.3.1 to 3.3.3.

3.3.1 Equation Error Method

The Equation Error Method (EEM) is based on the Least–Squares model, which was perhaps the first approach to the concept of optimality. The Least–Squares technique is mainly known in its application to the curve fitting or regression analysis. In these problems it is desired to represent the measured data by simple functional relationship or by a smooth curve. The solution minimizes the sum of the squares of deviations between data points and corresponding points obtained from the solution.

Measurement vector consists of the output vector and measurement noise $\vec{\nu}$:

$$\vec{z} = \vec{y} + \vec{\nu} \tag{3.32}$$

Simplification of the dynamic system equations to linear combination of regressors to:

$$\vec{y} = \boldsymbol{X}\,\vec{\theta} \tag{3.33}$$

where $\boldsymbol{X}$ is the matrix of regressors.

Ordinary Least–Squares (OLS) model is well–known estimation model. Model is assumption free, so no a–priori known probability densities of $p\left(\vec{\theta}\right)$ and $p\left(\vec{\nu}\right)$ are required. OLS is sometimes called just a Least–Squares. Model uses cost function expressed as a sum of squares [25]:

$$J\left(\vec{\theta}\right) = \frac{1}{2}\left(\vec{z} - \boldsymbol{X}\vec{\theta}\right)^T\left(\vec{z} - \boldsymbol{X}\vec{\theta}\right) \tag{3.34}$$

Generalization of the Ordinary Least–Squares to Weighted Least–Squares (WLS) uses inversion of weight matrix $\boldsymbol{R}^{-1}$ and cost function became to:

$$J\left(\vec{\theta}\right) = \frac{1}{2}\left(\vec{z} - \boldsymbol{X}\vec{\theta}\right)^T\boldsymbol{R}^{-1}\left(\vec{z} - \boldsymbol{X}\vec{\theta}\right) \tag{3.35}$$

The extension of the Least–Squares technique to the estimation of parameters of the dynamic system from measured time histories of the input and output is based on the assumption:

$$\vec{y} = \dot{\vec{x}} \tag{3.36}$$

Using this assumption measured output $\vec{z}$ is equal to:

$$\vec{z} = \dot{\vec{x}} + \vec{\nu} \tag{3.37}$$

Given that:

- $\vec{x}$ and $\vec{u}$ are known from the measurements without errors; and
- $\vec{z}$ are measured values, corrupted by measurement errors.

Using the measured data and above mentioned equations, the resultant aerodynamic forces and moments acting on the airplane are expressed by means of the aerodynamic model equations which may be written as

$$\dot{\vec{x}} = \theta_0 + \theta_1\, \vec{x}_1 + \cdots + \theta_n\, \vec{x}_n + \theta_{n+1}\, \vec{u} + \cdots + \theta_{n+m}\, \vec{u}_m \tag{3.38}$$

In this equation $\dot{\vec{x}}$ represents the resultant coefficient of the aerodynamic force or moment, θ_1 through θ_{n+m} are the stability and control derivatives, θ_0 is the value of any particular coefficient corresponding to the initial steady-state flight conditions, $\vec{x}_1$ to $\vec{x}_n$ are the airplane states, and $\vec{u}_1$ to $\vec{u}_m$ are the control variables.

By substituting $\vec{y}$ in Equation 3.38 the measured values of x and u could be taken into form of Equation 3.33. Then the equation error can be expresses as:

$$\vec{\nu} = \vec{z} - \boldsymbol{X}\vec{\theta} \tag{3.39}$$

where:

$$\boldsymbol{X} = [1,\ \vec{x}_1,\ \ldots,\ \vec{x}_n,\ \vec{u}_1,\ \ldots,\ \vec{u}_m] \tag{3.40a}$$

$$\vec{\theta} = [\theta_0,\ \theta_1,\ \ldots,\ \theta_{n+m}]^T \tag{3.40b}$$

The minimization of the cost function 3.34:

$$J(\vec{\theta}) = \frac{1}{2}\left(\vec{z} - \boldsymbol{X}\vec{\theta}\right)^T \left(\vec{z} - \boldsymbol{X}\vec{\theta}\right) \tag{3.41}$$

is obtained by setting

$$\frac{\partial J(\vec{\theta})}{\partial \theta} = 0 \tag{3.42}$$

Because of

$$\frac{\partial J\left(\hat{\vec{\theta}}\right)}{\partial \vec{\theta}} = -\boldsymbol{X}^T\left(\vec{z} - \boldsymbol{X}\hat{\vec{\theta}}\right) = 0 \tag{3.43}$$

then $\hat{\vec{\theta}}$ can be solved as

$$\hat{\vec{\theta}} = \left(\boldsymbol{X}^T\boldsymbol{X}\right)^{-1}\boldsymbol{X}^T\vec{z} \tag{3.44}$$

This result is called the Least–Square estimate of $\vec{\theta}$.

The estimation of longitudinal motion model parameters utilizes a linear model structure described in Equation 2.78. As an example for parameter estimation, the velocity can be used. In this case the vectors of parameters, regressors are defined as follows:

$$\boldsymbol{X} = \left[\vec{V},\ \vec{\alpha},\ \vec{q},\ \vec{\theta},\ \vec{\delta_e},\ \vec{F_P}\right] \tag{3.45a}$$

$$\vec{\theta} = \left[D_V,\ D_\alpha,\ D_q,\ D_\theta,\ D_{\delta_e},\ D_{F_P}\right]^T \tag{3.45b}$$

The derivative of velocity was numerically computed using the smoothed local numerical differentiation and it is considered as the left side of Equation 3.38. Both regressor and derivative are substituted into Equation 3.44.

The identified model in a state–space representation has certain advantages e.g. it is possible to use it for a stability analysis, express dynamic characteristic of the system. In some cases it can be useful to express the aerodynamic derivatives directly. This approach requires to compute the forces and moments acting on the aircraft according to Equation 2.61 and Equation 2.65:

$$X = m\ (\dot{u} + G_0\ \sin\theta - r\,v + q\,w) \tag{3.46a}$$

$$Y = m\ (\dot{v} - G_0\ \cos\theta\sin\phi - p\,w + r\,u) \tag{3.46b}$$

$$Z = m\ (\dot{w} - G_0\ \cos\theta\cos\phi - q\,u + p\,v) \tag{3.46c}$$

$$L = J_x\,\dot{p} - J_{xz}\,\dot{r} + q\,r\left(J_z - J_y\right) - p\,q\,J_{xz} \tag{3.46d}$$

$$M = J_y\,\dot{q} + p\,r\,(J_x - J_z) + J_{xz}\left(p^2 - r^2\right) \tag{3.46e}$$

$$N = -J_{xz}\,\dot{p} + J_z\,\dot{r} + p\,q\left(J_y - J_x\right) + q\,r\,J_{xz} \tag{3.46f}$$

and express the forces and moments coefficients in body fixed frame as follows:

$$C_X = \frac{m\ (\dot{u} + G_0\ \sin\theta - r\,v + q\,w)}{\bar{q}\,S} \tag{3.47a}$$

$$C_Y = \frac{m\ (\dot{v} - G_0\ \cos\theta\sin\phi - p\,w + r\,u)}{\bar{q}\,S} \tag{3.47b}$$

$$C_Z = \frac{m\ (\dot{w} - G_0\ \cos\theta\cos\phi - q\,u + p\,v)}{\bar{q}\,S} \tag{3.47c}$$

$$C_l = \frac{J_x\,\dot{p} - J_{xz}\,\dot{r} + q\,r\left(J_z - J_y\right) - p\,q\,J_{xz}}{\bar{q}\,S\,b_w} \tag{3.47d}$$

$$C_m = \frac{J_y\,\dot{q} + p\,r\,(J_x - J_z) + J_{xz}\,(p^2 - r^2)}{\bar{q}\,S\,\bar{c}} \tag{3.47e}$$

$$C_n = \frac{-J_{xz}\,\dot{p} + J_z\,\dot{r} + p\,q\left(J_y - J_x\right) + q\,r\,J_{xz}}{\bar{q}\,S\,b_w} \tag{3.47f}$$

In this case the model for parameter estimation is inspired by the aerodynamic model from Equations 2.46, the only difference is that it is necessary to add the effect of the aircraft propulsion. The regressor and parameter vectors are expressed as follows:

$$\boldsymbol{X} = \left[1,\ \vec{V},\ \vec{\alpha},\ \vec{q}^{*},\ \vec{\delta_e},\ \vec{F_P}\right] \tag{3.48a}$$

$$\vec{\theta} = \left[C_{Xb},\ C_{X\alpha},\ C_{Xq},\ C_{X\delta_e},\ C_{XF_P}\right]^T \tag{3.48b}$$

where the forces and moments coefficients are taken as the left side of the regression model described in Equation 3.38. Direct computation of aerodynamic coefficients can be beneficial for building the dynamic model of the examined aircraft or aerodynamic analysis.

3.3.2 Output Error Method

The Output Error Method (OEM) belongs to the category of the maximum likelihood parameter estimators and it is a widely used technique in the field of aircraft parameters estimation. The advantage of this approach is in its simple utilization for systems with nonlinear dynamics. The necessity of the initial parameters estimate can be taken as a minor drawback, the OEM is thus assumed as the algorithm for initial model improvement according to real measurement.

The OEM parameter estimator was designed for the Fisher model structure, that can be considered in either linear or nonlinear form and is described in Equations (3.49). The uncertainties are based on a–priori knowledge of the measurement noise $\vec{\nu}$.

$$\vec{z} = \boldsymbol{H}\vec{\theta} + \vec{\nu} \tag{3.49a}$$

$$\vec{z} = h\left(\vec{\theta}\right) + \vec{\nu} \tag{3.49b}$$

The measurement noise $\vec{\nu}$ has the normal distribution defined as:

$$\vec{\nu} \quad \sim \quad \mathbb{N}\left(0, \boldsymbol{R}\right) \tag{3.50}$$

In practical applications the noise covariance matrix is usually estimated from measurement noise $\vec{\nu} = \vec{y} - h\left(\vec{\theta}\right)$. The estimation process is shown in the following equation.

$$\hat{\boldsymbol{R}} = \frac{1}{N}\sum_{i=1}^{N} \vec{\nu}\left(i\right)\vec{\nu}^T\left(i\right) \tag{3.51}$$

Using the property of normal distribution from Equation 3.5: $p\left(\vec{z}\middle|\vec{\theta}\right)$ is defined as:

$$p\left(\vec{z}\middle|\vec{\theta}\right) = \frac{1}{\sqrt{\left(2\pi\right)^{n_z}\ \det\left(\boldsymbol{R}\right)}} \exp\left(-\frac{1}{2}\left(\vec{z} - \boldsymbol{X}\vec{\theta}\right)^T \boldsymbol{R}^{-1}\left(\vec{z} - \boldsymbol{X}\vec{\theta}\right)\right) \tag{3.52}$$

where n_z is the number of measured variables in $\vec{z}$.

The likelihood function is considered to have normal distribution, thus it is possible to express it as the conditioned probability function from foregoing equation. The Fisher model is based on the Fisher estimation theory using:

$$\mathbb{L}\left(\vec{z};\vec{\theta}\right) = p\left(\vec{z}\middle|\vec{\theta}\right) \tag{3.53}$$

The maximum likelihood estimator that is recommended for the linear form of the Fisher model searches a maximum of the following likelihood function.

$$\mathbb{L}\left(\vec{z};\vec{\theta}\right) = \frac{1}{\sqrt{(2\pi)^{n_z}\,\det\left(\boldsymbol{R}\right)}}\,\exp\left(-\frac{1}{2}\left(\vec{z}-\boldsymbol{X}\vec{\theta}\right)^T\boldsymbol{R}^{-1}\left(\vec{z}-\boldsymbol{X}\vec{\theta}\right)\right) \tag{3.54}$$

Therefore the parameter estimate $\hat{\vec{\theta}}$ can be expressed as:

$$\hat{\vec{\theta}} = \max_{\vec{\theta}}\mathbb{L}\left(\vec{z};\vec{\theta}\right) \tag{3.55}$$

The maximum of the likelihood function is found with the utilization of logarithm and the becoming a negative log–likelihood.

$$-\ln\left[\mathbb{L}\left(\vec{z};\vec{\theta}\right)\right] = \frac{1}{2}\left(\vec{z}-\boldsymbol{X}\vec{\theta}\right)^T\boldsymbol{R}^{-1}\left(\vec{z}-\boldsymbol{X}\vec{\theta}\right)+\frac{1}{2}\ln\left[\det\left(\boldsymbol{R}\right)\right] \tag{3.56}$$

Using known measurement noise covariance matrix cost function became:

$$J\left(\vec{\theta}\right) = \frac{1}{2}\left(\vec{z}-\boldsymbol{X}\vec{\theta}\right)^T\boldsymbol{R}^{-1}\left(\vec{z}-\boldsymbol{X}\vec{\theta}\right) \tag{3.57}$$

The cost function for minimization is equal to Weighted Least–Squares.

Using the estimation of measurement noise covariance matrix from Equation 3.51, the cost function with omitted constant terms becames:

$$J\left(\vec{\theta}\right) = \frac{1}{2}\ln\left[\det\left(\boldsymbol{R}\right)\right] \tag{3.58}$$

The Output Error Method (OEM) minimizes the errors between the actual output and the model output by using the same input. It is assumed that only measured outputs are corrupted by noise and that there are no gust or other disturbances to the airplane. The optimization problem, involved is nonlinear and requires the use of an iterative solution. The Modified Newton–Raphson (MNR) technique is usually applied because of its good convergence rate even for large number of unknown parameters. The OEM is also called the maximum likelihood method because Fisher model is used for the parameter estimation in the output error cost function.

Linear OEM is based on the linear system described in Equations 2.70 and the measured output is corrupted by error. Using this assumption measured output $\vec{z}$ is equal to:

$$\vec{z} = \dot{\vec{x}} + \vec{\nu} \tag{3.59}$$

The vector of unknown parameters include, in general, the elements of all matrices in the model equations and the initial conditions. As indicated in the reference [22], the minimization of the cost function with respect to the unknown parameters can be solved by several gradient–based nonlinear programming methods.

The iteration in these methods in general is given as:

$$\vec{\theta}_{r+1} = \vec{\theta}_r - c_r\,\boldsymbol{M}_{qr}^{-1}\,\boldsymbol{G}_r \tag{3.60}$$

where c_r is the scalar step size parameter in r^{th} iteration chosen to improve the convergence, $\boldsymbol{M}_{qr}$ is the information matrix in r^{th} iteration and $\boldsymbol{G}_r$ is the gradient matrix of the cost function in r^{th} iteration.

The gradient matrix of the cost function of Fisher model (see Equation 3.57) has the form:

$$\boldsymbol{G}_r = \left. \frac{\partial J\left(\vec{\theta}\right)}{\partial\left(\vec{\theta}\right)} \right|_{\vec{\theta}=\vec{\theta}_r} = \sum_{i=1}^{N} \boldsymbol{S}_i^T\left(\theta_r\right) \boldsymbol{R}^{-1} \left[z\left(i\right) - \hat{y}\left(i, \theta_r\right)\right] \tag{3.61}$$

where $\boldsymbol{S}$ is the sensitivity Jacobian matrix constructed as:

$$\boldsymbol{S} = \frac{\partial \vec{y}}{\partial \vec{\theta}} = \begin{bmatrix} \frac{\partial y_1}{\partial \theta_1} & \frac{\partial y_1}{\partial \theta_2} & \cdots & \frac{\partial y_1}{\partial \theta_{n_x}} \\ \frac{\partial y_2}{\partial \theta_1} & \frac{\partial y_2}{\partial \theta_2} & \cdots & \frac{\partial y_1}{\partial \theta_{n_x}} \\ \vdots & \vdots & \ddots & \vdots \\ \frac{\partial y_{n_x}}{\partial \theta_1} & \frac{\partial y_{n_x}}{\partial \theta_2} & \cdots & \frac{\partial y_{n_x}}{\partial \theta_{n_x}} \end{bmatrix} \tag{3.62}$$

The output sensitivities were numerically computed with utilization of central finite differences.

$$\frac{\partial \vec{y}}{\partial \theta_j} = \frac{\hat{y}\left(\vec{\theta} + \delta\vec{\theta}_j\right) - \hat{y}\left(\vec{\theta} - \delta\vec{\theta}_j\right)}{2\left|\delta\vec{\theta}_j\right|} \tag{3.63}$$

where $\delta\vec{\theta}_j$ is the vector of pertuberation of parameter $j = 1, \ldots, n_\theta$ with other parameters equal to zero. For the purposes of this thesis, the magnitude of pertuberation $|\delta\vec{\theta}_j|$ is equal to 10^{-3}.

The Fischer information matrix $\boldsymbol{M}_{qr}$ for the Modified Newton–Raphson method is approximated as

$$\boldsymbol{M}_{qr} = \sum_{i=1}^{N} \boldsymbol{S}_i^T\left(\vec{\theta}_r\right) \boldsymbol{R}^{-1} \boldsymbol{S}_i\left(\vec{\theta}_r\right) \tag{3.64}$$

The OEM with the Modified Newton–Raphson algorithm was introduced in [25, 22] and it has been used extensively for the past several years. It usually takes the results from the EEM as the initial values for the parameter estimates. As long as the method is applied to linear flight regimes or where the form of equations is known, it works very well. The disadvantage of the OEM is in the degradation of the results in the presence of the process noise. This may result in the computer program not converging or in poor estimates with large variances and or high correlation coefficients.

Another approach of computing the information matrix that can improve the bad conditioning and which can give more reasonable inverse is the Levenberg–Marquardt method.

Information matrix computed using Equation 3.64 is improved using following equation:

$$\boldsymbol{M}_q^{-1} = \left(\boldsymbol{M}_{q0} + \lambda \boldsymbol{I}\right)^{-1} \tag{3.65}$$

where λ is a positive nonzero scalar parameter. The initial value of λ is taken equal to 10^{-3}. As λ increases, Levenberg–Marquardt method starts to follow the cost gradient vector.

3.3.3 Recursive Least–Squares

Previous mentioned methods (EEM and OEM) are one step identification methods, that process all measured data in one step and determine parameters of modeled dynamic system, this approach is usually called offline identification. Recursive Least–Squares (RLS) algorithm process the data recursively over time, the term online identification is used in this case. It means that parameter estimate $\hat{\theta}(t)$ is computed partly from estimate in time $t-1$ and new information.

The recursive identification algorithms in general have following important features:

- They are the core part of adaptive algorithms employed in automatic control or signal processing.
- The memory requirements are much lower when compared to the one step methods.
- They are a suitable approach for online parameter identification.
- They are a part of algorithms for major fault or change detection at observed system.

Recursive Least–Squares method is based on reformulation of EEM to recursive form [25]. New parameter estimate $\vec{\theta}_{r+1}$ is defined as:

$$\vec{\theta}_{r+1} = \vec{\theta}_r + \boldsymbol{K}_{r+1}\left(\vec{z}_{r+1} - \vec{x}^T_{r+1}\vec{\theta}_r\right) \tag{3.66}$$

where $\boldsymbol{K}_{r+1}$ is the update gain matrix defined as:

$$\boldsymbol{K}_{r+1} = \boldsymbol{P}_r\,\vec{x}_{r+1}\left(\frac{1}{a} + \vec{x}^T_{r+1}\,\boldsymbol{P}_r\,\vec{x}_{r+1}\right)^{-1} \tag{3.67}$$

where a is the forgetting factor and $\boldsymbol{P}_r$ is a state covariance matrix. The forgetting factor can range from 0 (which means remember nothing) to 1 (which means no forgetting).

Update of covariance $\boldsymbol{P}_{r+1}$ is defined as:

$$\boldsymbol{P}_{r+1} = \boldsymbol{P}_r - \boldsymbol{K}_{r+1}\,\vec{x}^T_{r+1}\,\boldsymbol{P}_r \tag{3.68}$$

The forgetting factor enhance capability of the RLS to cope with time variant parameters. This approach will perform well when parameters are changing slowly, e.g., change of air density due to change of flight altitude. Quick changes of parameters due to structural changes cannot be followed. Therefore an adaptive Recursive Least–Squares parameter estimation is introduced.

Adaptive Recursive Least–Squares uses estimation of variance $\boldsymbol{V}$ to work with sudden changes of system:

$$\boldsymbol{V}_{r+1} = \frac{1}{N}\sum_{i=1}^{N}\left(\vec{z}_{r-i+1} - \vec{x}^T_{r-i+1}\vec{\theta}_{r-i}\right)^2 \tag{3.69}$$

where N is size of window for variance estimation.

Update gain matrix is then reformulated as:

$$\boldsymbol{K}_{r+1} = \boldsymbol{P}_r\,\vec{x}_{r+1}\boldsymbol{V}^{-1}_{r+1} \tag{3.70}$$

4. Experimenal results

This chapter contains description of the conducted flight experiments. Firstly, the used airplane is described in detail. Secondly, it is necessary to describe the used sensors, Data Acquisition System and the Primary Flight Display, which were used during the flight experiments. Thirdly, the flight maneuvers, the flight campaign and results of the Flight Path Reconstruction process will be introduced. Fourthly, the a–priori values of the investigated flight parameters are presented. Fifthly, the estimated flight parameters are presented. Finally, the summary of a–priori values and estimated flight parameters is given.

4.1 Research airplane

For the purposes of flight tests, the Evektor SportStar RTC[1] [12] airplane was used. Evektor SportStar RTC is an experimental Light Sport Airplane (CS-LSA certified) manufactured by Evektor–Aerotechnik, a.s. The photography of this airplane can be seen in Figure 4.1.

Figure 4.1: Photography of the experimental airplane.

4.1.1 Description of the airplane

The experimental airplane Evektor SportStar RTC is a two–seater airplane. Crew consists of a qualified test pilot from Evektor s.r.o. and flight engineer from Brno University of Technology.

Evektor SportStar RTC has a robust all metal airframe made of anodized duraluminum. The undercarriage consist of a three wheel fixed landing gear with steerable nose wheel and two main landing gear wheels equipped with hydraulic brakes. The airplane is configured as low–wing with conventional tail unit. To increase the safety of the flight crew in accordance to the modern trends is the aircraft equipped with a parachute rescue system [12].

[1]RTC – Restricted Type Certificate

The airplane is controlled via dual control stick and rudder pedal installation. There are three main control surfaces on this airplane: elevator with a trim surface, ailerons with trim surface on the left aileron, and rudder without an active trim surface. Flaps are electrically operated (lever on dashboard) and enable to be set to four positions: cruise position 0°, take–off position 15° and two landing positions 30° and 50°. This airplane does not have any air–brakes or spoilers. Deflections of all control surfaces of the Evektor SportStar RTC are given in Table 4.1.

Table 4.1: Control surface deflections of Evektor SportStar RTC [9].

Parameter	**Notation**	**Value**
Elevator	δ_e	$[-25°, +20°]$
Ailerons	δ_a	$[-17.5°, 17.5°]$
Rudder	δ_r	$[-30°, 30°]$
Elevator trim	δ_{te}	$[-5°, +25°]$
Aileron trim	δ_{ta}	$[-15°, +20°]$
Flaps	δ_f	$0°, 15°, 30°, 50°$

Evektor SportStar RTC uses the Bombardier Rotax 912ULS engine, which is an internal combustion piston engine with four stroke cycle, four horizontally opposed cylinders and reduction gearbox. Its fuel tanks have a volume of 60 liters in each wing. The engine is designed to use Unleaded fuel RON[2] 95. The airplane uses a 3–blade composite propeller of type WOODCOMP KLASSIC 170/3/R. This type of propeller is ground adjustable with a fixed pitch setting for the flight.

As it is not convenient directly measure the propeller rotational speed, it is proposed to be beneficial to measure the engine crankshaft speed and to divide the obtained value by reduction ratio. The propulsion parameters can be found in Table 4.2.

Table 4.2: Propulsion parameters [6, 23].

Parameter	**Notation**	**Value**
Engine reduction ratio	n	2.43
Propeller diameter	D_P	$1.7\,m$
Engine maximum torque	—	$128\,Nm$
Engine take–off power	—	$73.5\,kW$

The tactical data of the airplane, based on [23], are given in Table 4.3.

[2]RON –Research Octane Number

Table 4.3: Tactical data of Evektor SportStar RTC [12, 23].

Parameter	Notation	Value
Length of airplane	—	$5.98\,m$
Height of airplane	—	$2.48\,m$
Reference wingspan	b_w	$8.65\,m$
Reference wing area	S	$10.6\,m^2$
Length of MAC	$\bar{c}$	$1.25\,m$
Never exceed speed	V_{NE}	$75\,m/s$
Maximum flap extended speed	V_{FE}	$36\,m/s$
Maximum level speed	V_H	$59\,m/s$
Stall speed	V_{S1}	$20.6\,m/s$
Service ceiling	H_{max}	$4720\,m$

4.1.2 Flight envelope

The flight envelope describes the limits of flight. The limitations originate from different sources such as engine power, maximum speed, stall speed, service ceiling etc.

For the purposes of the flight tests, the flight envelope was limited to the conditions, as altitudes, airspeed and position of center of mass, as consulted with the airplane manufacturer. The limits reflect the safety constraints to prevent extreme attitudes.

The operational flight envelope and point of testing are presented in Figure 4.2.

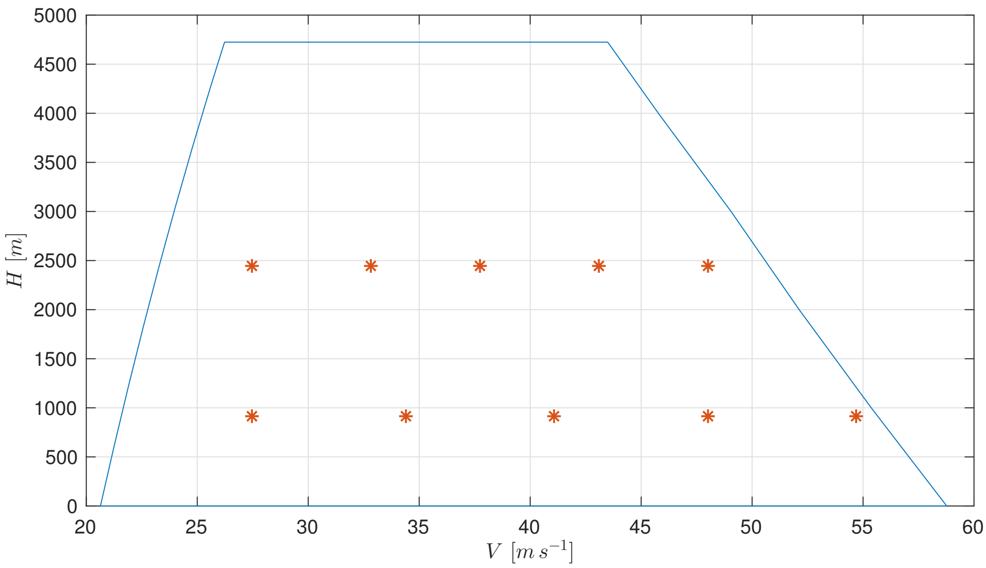

Figure 4.2: Operational flight envelope, the blue area denotes the envelope and red stars show the testing points.

4.1.3 Airplane's center of mass

The mass and the center of mass of the empty airplane was determined experimentally. First, it was necessary to empty the fuel tanks. Then, every wheel of the landing gear was put on a weighing scale. For this purpose, three weighing scales Soehnle Professional Digital Indicators 2755 were used. Next, it was necessary to put small blocks under the main wheels to ensure that the base plane of fuselage is horizontal, i.e., parallel to the floor.

After that, it was possible to start the measurement. To ensure the high accuracy of the results, five measurements was taken for each case. These measurements were used not only for determining the total mass of the empty airplane, but also to find the horizontal position of the center of mass of the empty airplane in the $x_d y_d$ plane.

The mass of the empty airplane was calculated to be $m_{empty} = 375\,kg$. It is necessary to say, that the measured airplane had a unique configuration and built–in parachute system, several sensor systems, including wiring, therefore the above mentioned mass of the empty airplane is unique for this particular experimental airplane and it cannot be compared to another unit of the same type.

The position of the center of mass of the empty airplane in Design reference frame was calculated using following formulas:

$$x_{Gd} = \frac{m_F\, x_{Fd} + m_L\, x_{Ld} + m_R\, x_{Rd}}{m_{empty}} \tag{4.1}$$

$$y_{Gd} = \frac{m_F\, y_{Fd} + m_L\, y_{Ld} + m_R\, y_{Rd}}{m_{empty}} \tag{4.2}$$

where F is the point of contact of front wheel with weighing scale, L is the point of contact of left wheel with weighing scale and R is the point of contact of right wheel with weighing scale.

At last, it was necessary to find the position of the center of mass of the empty airplane in the z_d axis. For this purpose, two laser distance sensors Leica Geosystems DISTO lite5 were attached to the airplane. Using these sensors the distance from placement of the sensors to the nearby vertical wall was measured several times. Firstly, one block was inserted under the front wheel to change tilt of the aircraft. Secondly, the laser distance sensors were used to measure distance from the same wall again to compute the angle of tilt. Finally, the distribution of mass on all three wheels was repeatedly measured. The whole process of inserting blocks below the front wheel, measuring distance from nearby wall and weighing of all three wheels was repeated three times to obtain sufficient quantity of data to determine position of center of mass in z_d axis. For this purpose, the following equation was used:

$$z_{Gd} = \frac{x_{G'd} - x_{Ld} + (x_{Ld} - x_{Gd}) \cos\theta}{\sin\theta} - z_{Ld} \tag{4.3}$$

where θ is tilt angle (pitch angle) and G' is projection of point G to the horizontal plane after tilting the airplane.

To obtain center of mass of the experimental airplane, it is necessary to take weight of the empty airplane and add the weight of other parts. Weights of the pilot and operator with their safety parachutes and the fuel weight are measured before every flight. Additional cargo was not present on–board during any of the experimental flights.

4.2 Instrumentation

During the test flights, the measured values of selected physical quantities were recorded. To collect and store measured data, a Data Acquisition System (DAQ) described in Section 4.2.1 was used. A list of on–board sensors is given in Section 4.2.2. To ensure that the conducted flight maneuver meet specified requirements, the Primary Flight Display (PFD) is used (see Section 4.2.3).

4.2.1 Data Acquisition System

The DAQ used to collect and store data from sensors was composed of selected modules of industrial CompactRIO[3] platform manufactured by National Instruments Corporation [34]. The flight ready DAQ was located in the cargo compartment of the experimental airplane and connected to a network of sensors (listed in following section). The DAQ was powered by a standalone battery power supply $24 - 28\,V$, as the experimental airplane was capable to provide only $12 - 14\,V$ from its engine–driven alternator.

The DAQ used in the flight tests is composed of following modules:

- **Real–Time Controller** NI[4] cRIO-9022 is powered by a $533\,MHz$ PowerPC processor and includes $256\,MiB$ DRAM[5] and $2\,GiB$ Solid–State Drive (SSD) for data storage. The Real–Time Controller controls other modules and can be programmed using the graphical programming system LabView.
- **CompactRIO Reconfigurable Chassis** NI cRIO-9114 can hold up to 8 modules. Only six slots were used for the purposes of flight tests. To sequence and synchronize these modules, Field–Programmable Gate Array (FPGA) Virtex–5 was used.
- **High–Speed CAN Module** NI 9862 provides an interface to the Controller Area Network (CAN) bus, which allows to connect devices with baud rate up to $1\,Mbps$ on the bus with a maximum length of $40\,m$.
- **Isolated Simultaneous Analog Input Module** (ISAIM) NI 9239 has 4 channels to connect the sensors having a signal range of $\pm 10\,V$ and an update rate of $50\,kS/s$. This module has 24–bit resolution which is required for critical sensors. It also has isolated inputs which reduce the risk of interferences and ground loops.
- **Universal Analog Input Module** (UAIM) NI 9219 has 4 channels to connect sensors having signal range of $\pm 10\,V$ and an update rate of $100\,S/s/ch$. This module has 24–bit resolution which is required for critical sensors. It also provides excitation current for potentiometers. For the purposes of the flight tests, three Universal Analog Input Modules are used.
- **Analog Input Module** (AIM) NI 9205 has 32 channels to connect sensors having update rate $250\,kS/s$. Each channel has configurable signal range from $\pm 200\,mV$ to $\pm 10\,V$. This module has 16–bit resolution which is sufficient for non–critical sensors.

[3] RIO – Reconfigurable Input/Output
[4] NI – National Instruments
[5] DRAM – Dynamic Random Access Memory

4.2.2 Utilized sensors

There are eight types of sensors which were connected to the Data Acquisition System during test flights: Xsens MTi–G, Integrated Flight State and Navigation Sensor (IFNS), potentiometers, strain gauge, flowmeter, flow vanes, pressure transducers and rotational speed sensors.

Xsens MTi–G sensor, manufactured by Xsens Technologies B.V. [50], integrates accelerometers, gyroscopes, GPS and magnetometers in its sensor fusion algorithms. The output of Xsens are Euler angles, specific forces, angular velocities, translational velocities and geodetic position in the WGS84. This sensor is connected to the DAQ using a RS-232 serial port interface. The Xsens sensor was placed in the cargo compartment behind the pilot's and operator's seats as this location was closest to the center of mass of the airplane.

Integrated Flight State and Navigation Sensor (IFNS), manufactured by Stock Flight Systems [42], integrates accelerometers, gyroscopes, GPS and magnetometers. Therefore the outputs of IFNS are Euler angles, specific forces, angular velocities, translational velocities and geodetic position in the WGS84 format. This sensor was connected using Controller Area Network (CAN) bus to the NI 9862 module. IFNS was placed in the cargo compartment behind the pilot's and operator's seats next to the Xsens sensor as this location is close to the center of mass of the airplane. IFNS was used as a secondary data source in case of the Xsens' malfunction.

Potentiometers SRS280[6], manufactured by Penny & Giles Controls Limited [35], were connected to the NI 9219 module. Potentiometers in above mentioned experimental airplane measure the position and orientation of the elevator, rudder, right aileron, flaps, pilot's control stick, throttle lever, and rudder pedals.

Strain gauges CEA-13-250UN-120, manufactured by Vishay Precision Group, Inc. [46], sense control forces. These strain gauges were mounted on the elevator and left aileron control rods, and on both rudder links. All strain gauges were wired as full Wheatstone bridges. They are connected thru a precision amplifier RM4220, manufactured by Hottinger Baldwin Messtechnik GmbH. [18], to the NI 9205 module.

Flowmeter Floscan 201B, manufactured by FloScan Instrument Co., Inc. [13], measured the fuel flow on the fuel line from fuel switch to the engine. This sensor was connected thru a pulse rate to analog converter IFMA 0035, manufactured by Red Lion Controls, Inc. [37], to the NI 9205 module. Flowmeter was attached near to the firewall.

Flow vanes were part of the SpaceAge 100400 Mini Air Data Boom (MADB), manufactured by the SpaceAge Control, Inc. [39], which was mounted on the right wing. Mini Air Data Boom was equipped with the angle–of–attack and flank angle flow vanes. Outputs from these flow vanes were connected to the NI 9219 module.

Pressure transducers DMP 331 and DPS+6, manufactured by the BD Sensors s.r.o. [4], were integrated for measurement of the static and impact pressure. They were connected to the pitot–static tube and to the NI 9239 module. The pitot–static tube is localed at the front part of the SpaceAge 100400 Mini Air Data Boom.

Rotational speed sensor was an integral part of the Bombardier Rotax engine [6]. It was

[6] SRS – Sealed Rotary Sensor

connected to the NI 9205 module. The rotational speed sensor was the measuring rotational speed of the engine crankshaft.

4.2.3 Primary Flight Display

Primary Flight Display – PFD was used to show graphs of selected physical quantities to ensure that the conducted flight maneuvers meet specified requirements (see next section). It was also used as a secondary flight recording system.

The PFD consists of a display, an ARM microprocessor with 512 MiB RAM[7] and 2 GiB Flash, and two buses – Ethernet bus and CAN bus. The display contains a Liquid Crystal Display (LCD) panel with Light–Emitting Diode (LED) backlight and a capacitive touch layer. The size of the display is 10" to increase the user–friendliness/readability of the whole system (and provide optimal performance even during difficult maneuvers).

On the back side of the PFD, there are six connectors (see Figure 4.3):

- Power input connector has three pins: common negative pin, positive battery pin for connecting 12 V backup battery and positive main power input pin. The main power input of the PFD is connected to the 14 V avionics bus thru the circuit breaker.
- Two CANbus connectors have integrated power output and support the CANaerospace protocol [**CANaerospace**]. Having two connecters enables a simultaneous connection of the IFNS and a second display for a more complex avionics solution.
- Ethernet connector is used to provide connection to the DAQ. Data coming thru Ethernet are presented on the PFD to ensure that the conducted flight maneuver meets specified requirements.
- The RS–232 connector is used as a debug interface for the PFD. A computer connected to the RS–232 connector is able to open a software terminal for managing the PFD software. Managing of PFD enables reading log messages, checking of the errors and warnings, and verification of the internal components of the PFD. RS–232 also enables to download logged records and an upload of new software versions.
- The auxiliary connector is used to connect up to 4 external buttons and an audio panel. Audio panel connection enables to send the audio information to the pilot's and operator's headphones.

The PFD was designed and developed at the Faculty of Information Technology. For the purposes of mounting the PFD on–board of the airplane, the airplane manufacturer equipped the experimental airplane with a custom dashboard containing prepared installation space according to the PFD specification.

The software for visualization of the flight maneuvers on the Primary Flight Display was programmed in LabView [33]. The LabView is a graphical system design software.

[7] RAM – Random Access Memory

(a) Front view (b) Rear view

Figure 4.3: Photography of the Primary Flight Display.

4.3 Flight data acquisition and preprocessing

The data were recorded during the flight experiments conducted on the experimental airplane Evektor SportStar RTC, owned by Evektor s.r.o., which operates an Authorized aircraft testing laboratory (authorization № L-3-060 issued by Civil Aviation Authority of Czech Republic – CAA [44]). The experimental airplane was equipped with Data Acquisition System sensors and a Primary Flight Display, see Section 4.2.

Gathered data were post–processed using Flight Path Reconstruction.

4.3.1 Dynamic longitudinal stability

The reason behind the acquisition of the flight data is the estimation of dynamic longitudinal stability characteristics. This task is based on exciting the investigated airplane dynamic response in longitudinal motion.

For the excitation of the system's dynamic response, a doublet maneuver was used. The doublet is a suitable testing maneuver as high complex maneuvers like 3-2-1-1 have to be executed using an automatic flight control system and simple pulses do not fully excite dynamic modes of the aircraft [22].

After exciting a dynamic mode of motion with an input and removing the pilot from the control loop, the system can record an aircraft open loop motion. A physical system's dynamic stability analysis is concerned with the resulting time history of motion of a system when displaced from an equilibrium condition [45].

A sophisticated solution to the aircraft Equations of Motion with valid aerodynamic inputs can result in good theoretically obtained time histories. However, the fact remains that the only way to discover the aircraft's actual dynamic motion is to flight test and record its motion for analysis [45].

Before the maneuver, the pilot has to meet these conditions [23]:

- Airplane must fly straight, steady and horizontal, so roll angle and flight path angle must be smaller than 5°.
- Airplane must maintain specified airspeed and at a specified altitude.

- All forces on control stick must be trimmed, no additional force should appear on the control stick.
- Airplane must have specified weight and position of center of mass.
- Airplane must have specified position of flaps.

The maneuver is started at specified airspeeds ranging from $1.2\,V_{S1}$ to V_H, or $1.2\,V_{S1}$ to $V_{FE} - 15\%$ with extended flaps [23]. The maneuver is conducted by inducing a doublet by pushing and pulling the control stick, when subsequent elevator deflection introduce the longitudinal motion.

4.3.2 Flight campaign

During the flight campaign, seven flights were conducted in the period of July and August 2012. The weather conditions while testing were without significant wind or mechanical or thermal turbulence. Flights were conducted in altitudes of $915\,m$ and $2438\,m$ ($3000\,ft$ and $8000\,ft$). Three flights were conducted with a front center of gravity position, two of them were conducted with "fixed control" after inducing the doublet maneuver and one of it was conducted with "free control". Another four flights were conducted at the rear center of gravity position. Two of the flights were conducted with a "fixed control" after inducing the doublet and two were conducted under "free control" conditions.

All flight tests were performed at a certified aerodrome in Kunovice. ICAO code of aerodrome is LKKU.

4.3.3 Flight Path Reconstruction

The Flight Path Reconstruction (FPR) post–processes the raw measured data. Angle–of–attack is being corrected for upwash effect described in Section 3.1.1. Specific forces and angle–of–attack are corrected for the position error using equations in Section 3.1.2. On the corrected data, Kalman Filter described in Section 3.1.4 is used to minimize the effects of measurement noise.

For the purposes of this thesis, the author has implemented the algorithm with all the corrections necessary. The Flight Path Reconstruction algorithm is implemented in Matlab [31].

An example of few chosen physical quantities during a flight maneuver is presented in Figure 4.4. Blue lines represent raw measured data and red lines represent data after the corrections and Flight Path Reconstruction.

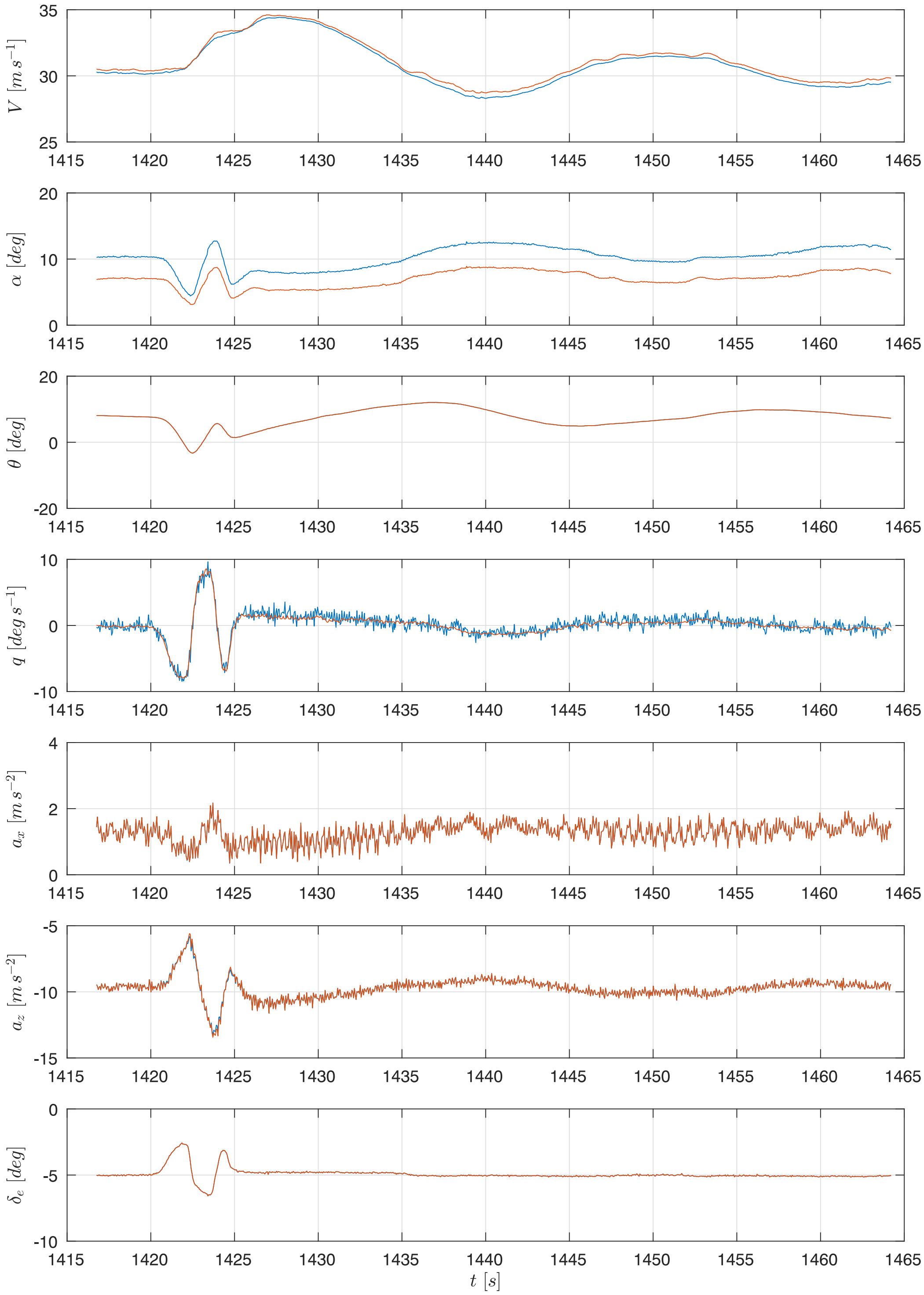

Figure 4.4: Comparison of the data before and after FPR process (Blue lines represents raw measured data and red lines represents data after FPR).

4.4 A–priori data

The a–priori data are the outputs from the softwares described in Section 3.2. All models used in this thesis are based on the information provided by the airplane manufacturer [23]. More information about the numerical models providing the flight parameters is introduced in following sections.

4.4.1 Tornado software estimates

For the purposes of obtaining the a–priori values from the Tornado software, the author has created a model of the investigated airplane based on the information provided by airplane manufacturer [23]. Picture of the airplane's model is presented in Figure 4.5.

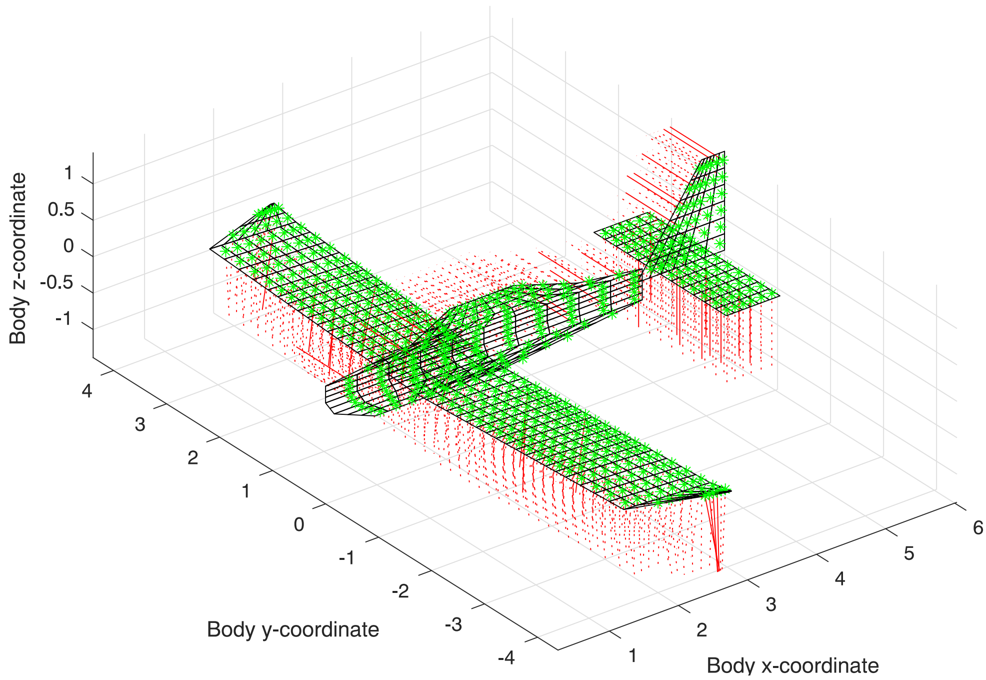

Figure 4.5: Airplane's model in Tornado software.

The model of the whole airplane has been split into panels of equal ratios. On the figure, the green stars show the position of the control points and the red dotted lines indicates the normals to each panel surface. The model coordinates are shown in the Design Reference Frame F_d.

The model consists of the wing, fuselage, vertical and horizontal tail units. The wing has been divided into 126 panels. The horizontal and vertical tail units are divided into 24 panels each. The fuselage is substituted by its planar projection, as Tornado does not support slender body modeling. The fuselage is divided into 130 panels.

4.4.2 AVL software estimates

For the purposes of obtaining a–priori values from the AVL software, the author has created a model of the investigated airplane based again on the information provided by the airplane manufacturer [23]. Picture of the AVL airplane model is shown in Figure 4.6.

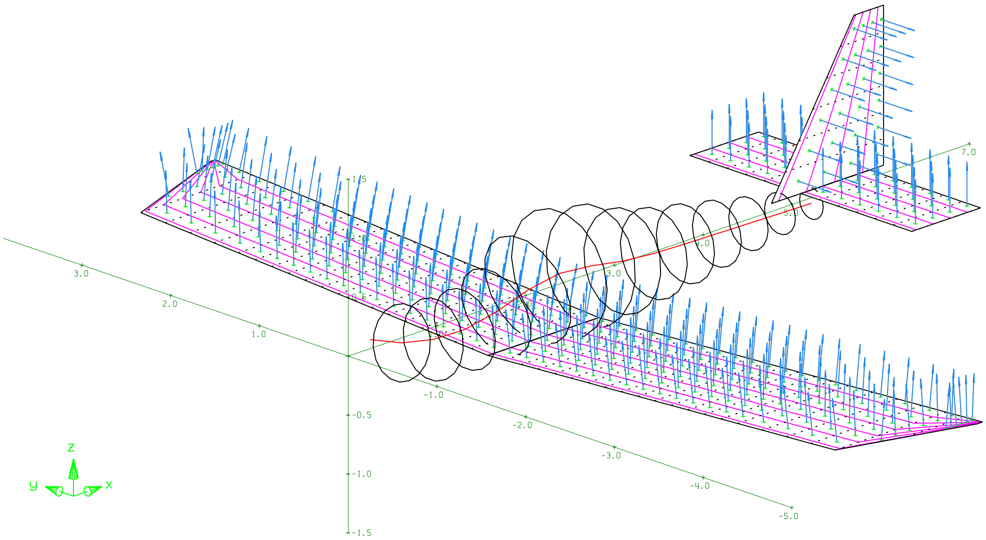

Figure 4.6: Airplane model in AVL software.

The model of the whole airplane has been split into panels of similar ratios. In the figure, the green stars show the position of the control points and the blue lines indicate the normals to each panel surface. The model coordinates are in the Design Reference Frame F_d.

The model same as in previous case, consists of the wing, fuselage, vertical and horizontal tail units. The wing has also been divided into 126 panels. The horizontal and vertical tail units feature 24 panels each. The shape of the fuselage is modeled using circles with the cross–section characteristics of the actual fuselage, hence AVL does not support fuselage fully. The fuselage has been divided into 15 parts by planes as shown in the Figure 4.6. The figure also show the red line indicating the center of the fuselage planes.

4.4.3 Datcom software estimates

A model of the experimental airplane was developed as a part of the "Smart Autopilot" project. It was based on the outputs of the USAF Datcom introduced in Section 3.2.3.

The model data from Datcom estimates are thoroughly described in [9].

4.5 Parameter estimation

The flight parameters were estimated using methods described in Section 3.3. The author's contribution is beyond other also in the software implementation of all three algorithms in Matlab [31]. Both nonlinear and linear Equations of Motion were considered. Using both modeling approaches allows for a straight forward comparison of both approaches.

All flight parameters introduced in Section 2.3.2 were divided into two main types: force parameters and moment parameters. For the purposes of this thesis, only the longitudinal parameters are presented.

4.5.1 Force parameters

The force parameters are independent of the center of mass position. The force longitudinal parameters can be divided to respective drag parameters C_{Dx} and lift parameters C_{Lx}.

The drag curve slope $C_{D\alpha}$ and lift curve slope $C_{L\alpha}$ define the basic performance of an airplane. Both of these flight parameters depend on the shape, size and aerodynamic characteristics of the airplane. The $C_{L\alpha}$ must be positive and its theoretical maximum is equal to 2π.

The flight parameter C_{L0} is equal to lift coefficient C_L in the case when the angle–of–attack α is equal to zero, elevator deflection δ_e is equal to zero and pitch rate q is equal zero.. Similarly, the flight parameter C_{D0} is equal to drag coefficient C_D in case the angle–of–attack α is equal zero and pitch rate q is equal zero.

Another lift parameter is the C_{Lq} (lift due to pitch rate) and $C_{L\delta_e}$ (elevator effect on lift). The C_{Lq} could be neglected, as the effect of this flight parameter on the lift coefficient C_L is very small. The flight parameter $C_{L\delta_e}$ depends on shape, size and characteristics of the elevator. The $C_{L\delta_e}$ must be positive for classical airframe configurations.

The drag parameters C_{Dq} (drag due to pitch rate) and $C_{D\delta_e}$ (elevator effect on drag) are neglected, as the effect of those flight parameters on drag coefficient C_D is very small.

The estimation results of the force parameters are shown in Figure 4.7. The lift parameters are compared to the a–priori values from the Tornado software, AVL software and Datcom. More details about the a–priori values are presented in Section 4.4.

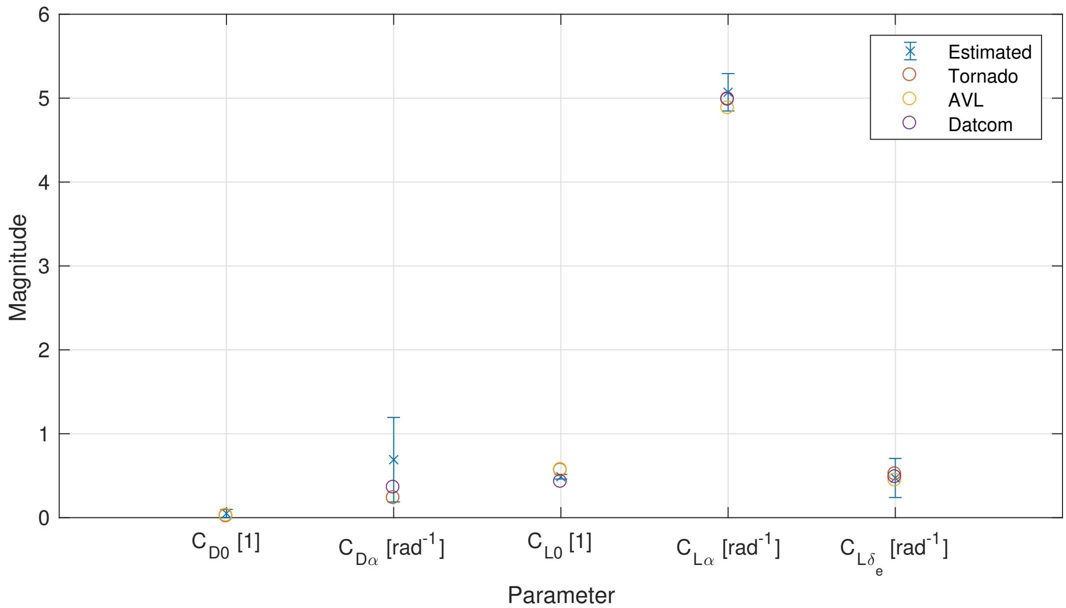

Figure 4.7: Graph of force parameters.

Figure 4.8 shows the dependence of the drag coefficient C_D whose Taylor's series expansion consist of the above discussed flight parameters (C_{Dx}) as a function of the angle–of–attack α. The blue stars show the data points from the identification maneuvers executed at altitude $915\,m$ ($3000\,ft$) and the red stars show the data points from the maneuvers performed at altitude $2438\,m$ ($8000\,ft$). The orange line presents a linear interpolation of the dependence of drag coefficient C_D on the angle–of–attack α.

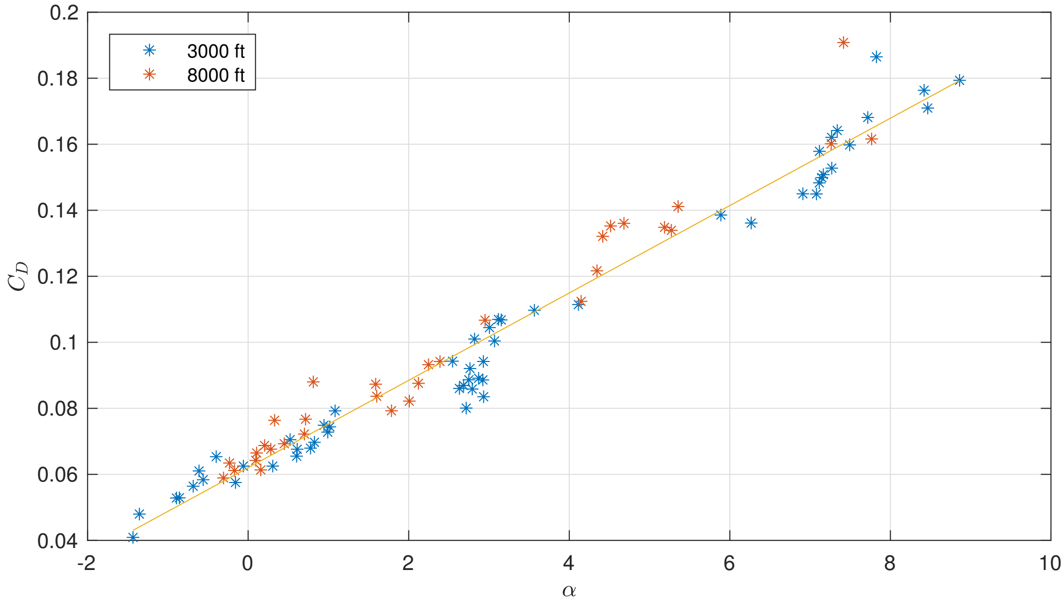

Figure 4.8: Graph of drag curve.

Figure 4.9 shows the dependence of the lift coefficient C_L whose Taylor's series expansion consist of the above discussed flight parameters (C_{Lx}) as a function of the angle–of–attack α.

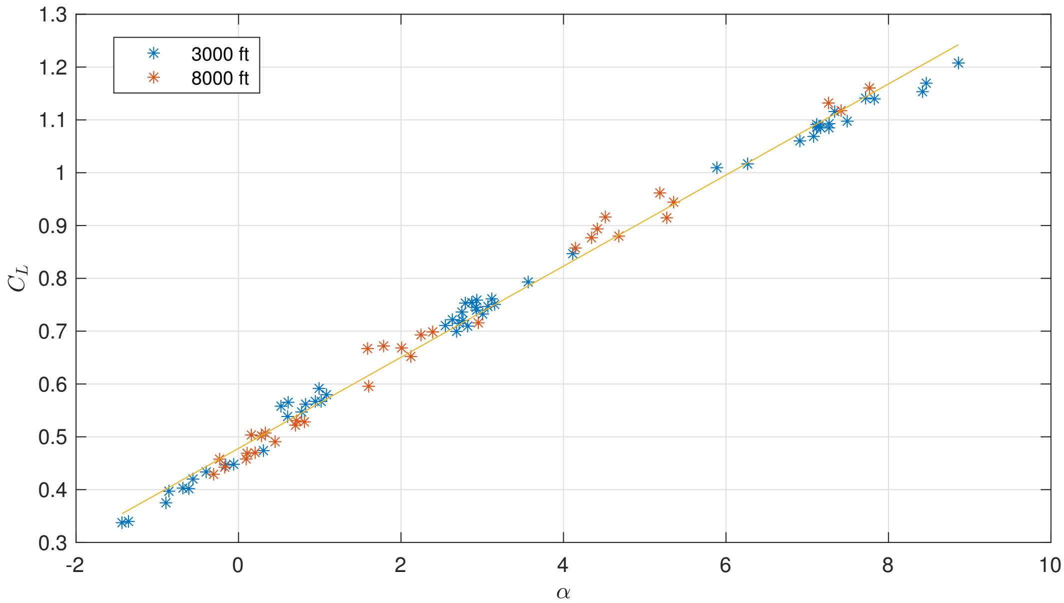

Figure 4.9: Graph of lift curve.

The blue stars show the data points from the maneuvers executed at altitude $915\,m$ ($3000\,ft$) and the red stars show the data points from the identification maneuvers executed at altitude $2438\,m$ ($8000\,ft$). The orange line presents a linear interpolation of the dependence of the lift coefficient C_L on the angle–of–attack α.

4.5.2 Moment parameters

The moment parameters depend on the center of mass position. The moment longitudinal parameters are the pitch moment parameters C_{mx}.

The pitching moment slope $C_{m\alpha}$ strongly depend on the center of mass position. The $C_{m\alpha}$ should be negative as it defines the level of static stability [11].

The flight parameter C_{m0} is equal to the pitch moment coefficient C_m in the case that the angle–of–attack α is equal to zero, pitch rate q is equal to zero and elevator deflection δ_e is equal to zero.

The pitch damping parameter C_{mq} specifies the dynamic longitudinal behavior of the airplane. The parameter C_{mq} must be negative, otherwise the airplane will be dynamically unstable.

The elevator effect on pitching moment $C_{m\delta_e}$ is the main control parameter in longitudinal motion. The flight parameter $C_{m\delta_e}$ depends on shape, size and characteristics of the elevator. The $C_{m\delta_e}$ should be negative for the classical tail configuration.

Results of the estimation of the moment parameters are presented in Figures 4.10 to 4.13. The position of the center of mass is expressed in a fraction of the Mean Aerodynamic Chord of main wing in percents.

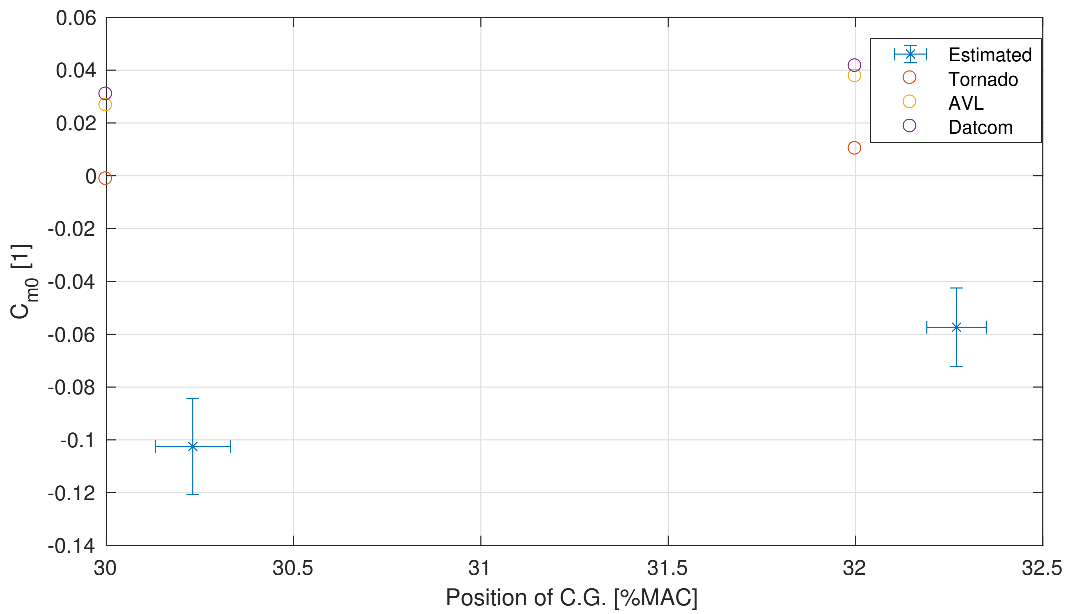

Figure 4.10: Graph of parameter C_{m0}.

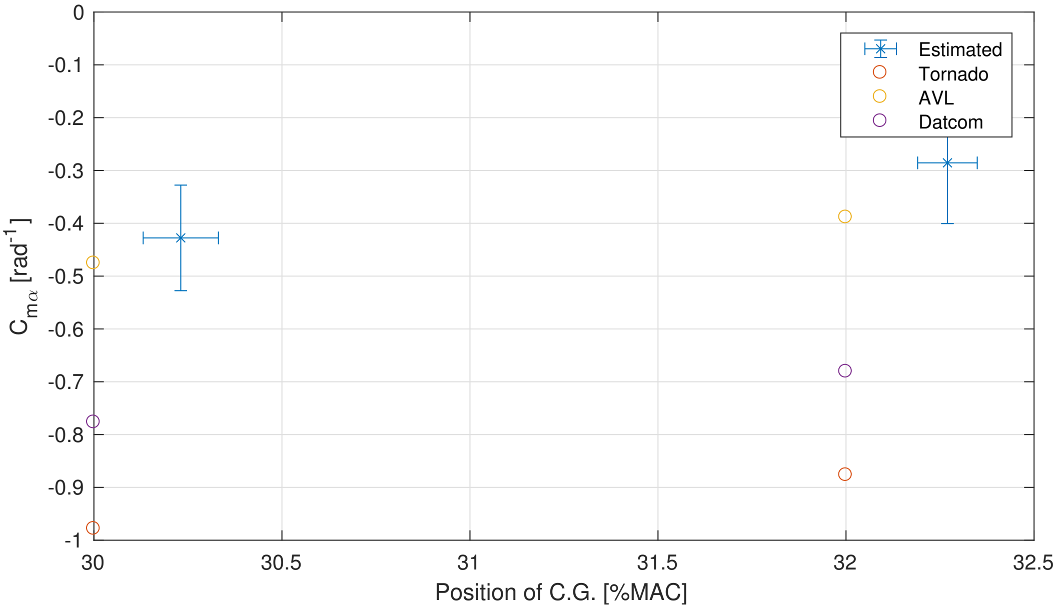

Figure 4.11: Graph of parameter $C_{m\alpha}$.

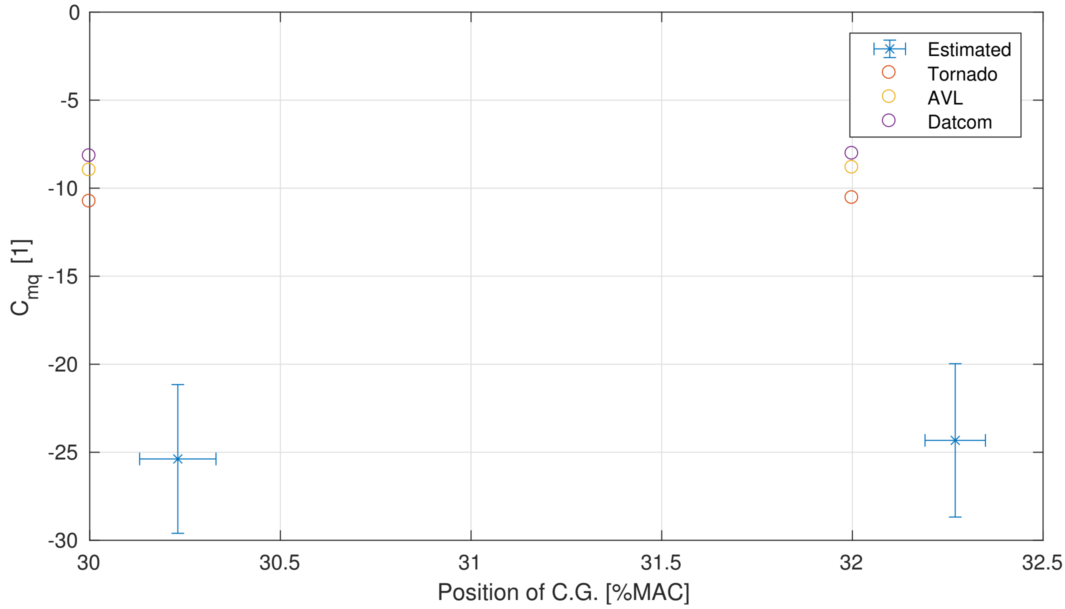

Figure 4.12: Graph of parameter C_{mq}.

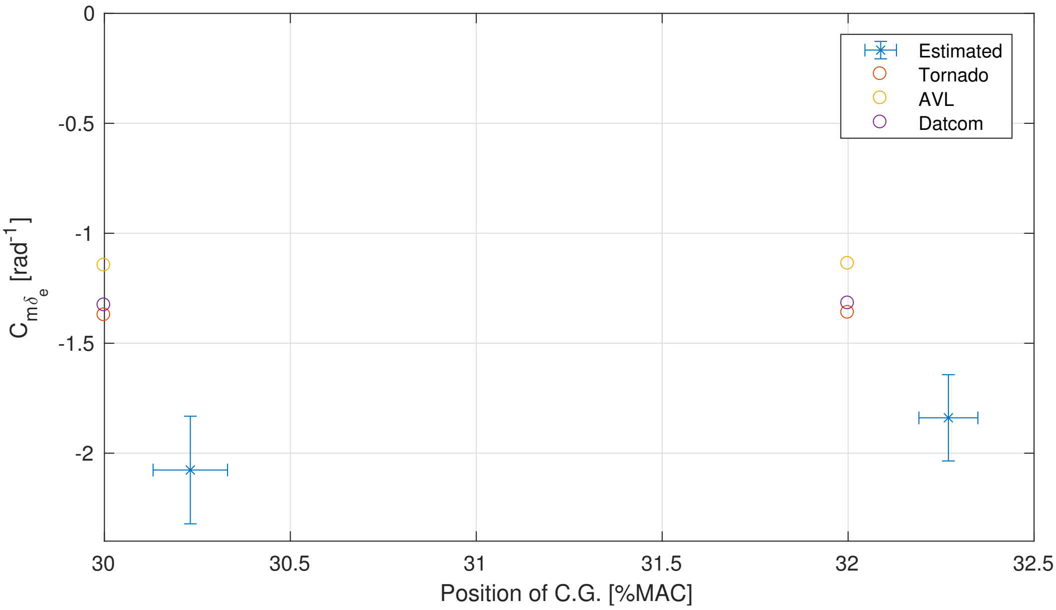

Figure 4.13: Graph of parameter $C_{m\delta_e}$.

4.5.3 Model validation

The dataset gathered during the flight campaign mentioned above was split into a training dataset and a validation dataset. The validation dataset contains the maneuvers used only for the validation of the estimated flight parameters. The estimated flight parameters were used for obtaining the simulated flight data. The simulation uses the input signal and initial conditions from the validation dataset. The outputs of the simulation were compared with measured flight data (see Figure 4.14).

The blue lines represents the measured flight data after the FPR process and the red lines represents the simulated flight data based on the estimated flight parameters. It can be seen in figure, that the airspeed V, angle–of–attack α, pitch angle θ and pitch rate q have a good fit. The translational accelerations a_x and a_z suffer from the vibrations caused by the 4 stroke combustion engine. As previously mentioned, an elevator doublet maneuver was used for the excitation. The elevator input is shown on last graph and does not contain a red line as the elevator is the input and thus it is not simulated.

After the comparison of the simulated and measured flight data it can be said that the simulated flight data based on the estimated flight parameters correspond sufficiently to the measured flight data. Therefore, it can be said, that the estimated flight parameters sufficiently describe the airplane aerodynamics and created model is sufficiently accurate.

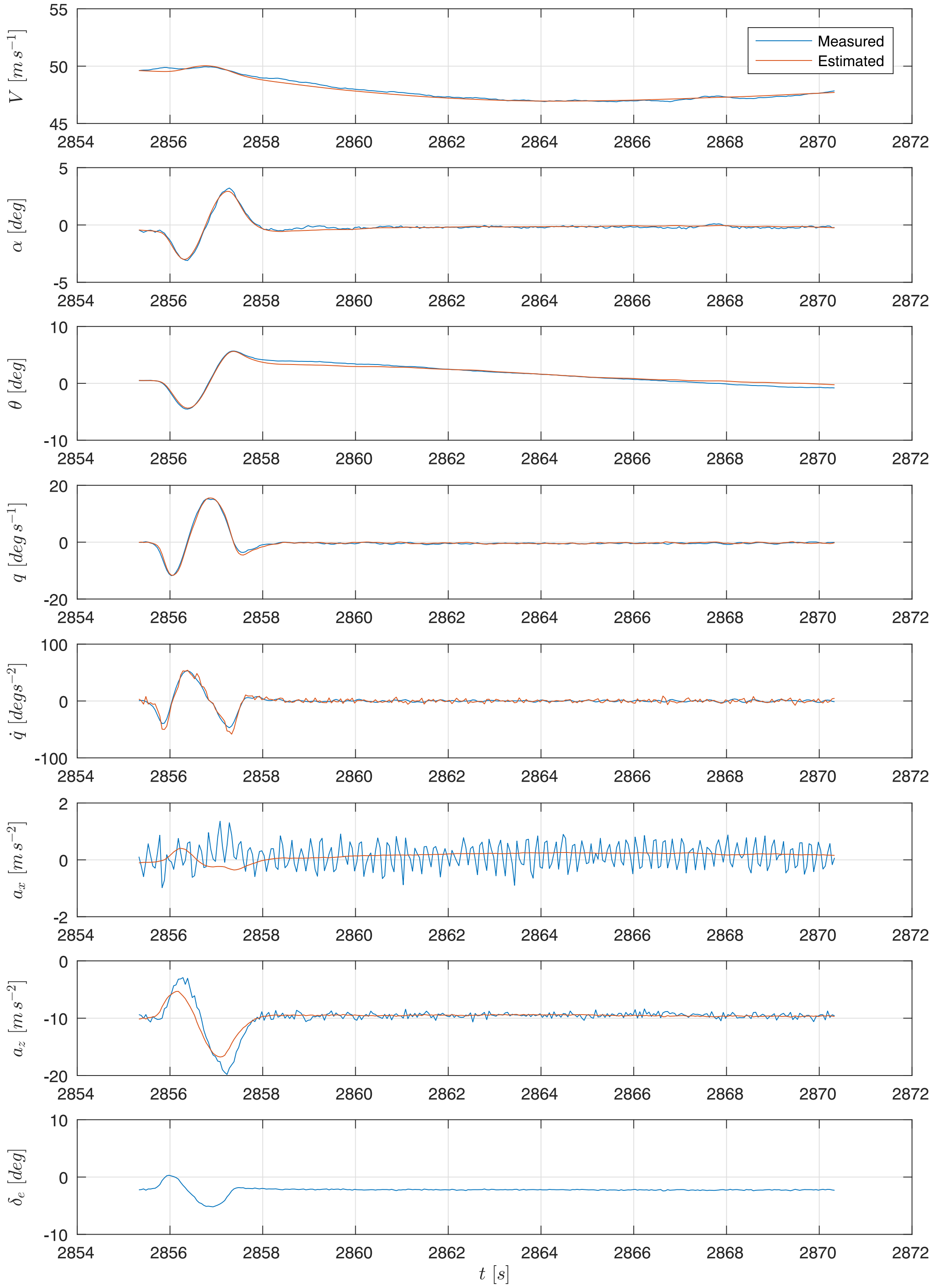

Figure 4.14: Recorded data for maneuver № 124.

4.6 Summary

All flight parameters of the experimental airplane, which were estimated from the measured flight test data fall within the limits presented in Sections 4.5.1 and 4.5.2.

4.6.1 Linear dependency of parameters

The linear characteristics of the force coefficients were presented in Section 4.5.1. The Figures 4.8 and 4.9 shows the selected part of the flight envelope and a linear interpolation of force coefficients.

4.6.2 Simulation and model validation

In Section 4.5.3, it was shown, that the simulated flight data based on the estimated flight parameters sufficiently correspond to the measured flight data. Therefore, it can be said, that the estimated flight parameters sufficiently describe the airplane aerodynamics and the created model is sufficiently accurate.

4.6.3 Correction of a–priori values

All sources of the a–priori aerodynamic coefficient values, exhibit difficulties with the drag flight parameters. The relative values of drag based flight parameters range within $[29\%, 52\%]$ of estimated flight parameters. The lift based flight parameters have a good a–priori prediction ranging within $[87\%, 117\%]$ of estimated flight parameters.

Table 4.4: Comparison of a–priori force parameters and force parameters obtained by estimation methods based on experimental flight data.

	Absolute values				Relative values			
Param.	**Est.**	**Tornado**	**AVL**	**Datcom**	**Est.**	**Tornado**	**AVL**	**Datcom**
C_{D0}	0.0510	0.0148	0.0244	—	1.00	0.29	0.48	—
$C_{D\alpha}$	0.6908	0.2326	—	0.3574	1.00	0.34	—	0.52
C_{L0}	0.4879	0.5619	0.5692	0.4256	1.00	1.15	1.17	0.87
$C_{L\alpha}$	5.0702	4.9873	4.8796	4.9805	1.00	0.98	0.96	0.98
$C_{L\delta_e}$	0.4730	0.5175	0.4419	0.4820	1.00	1.09	0.93	1.02

Table 4.5: Comparison of a–priori moment parameters and moment parameters obtained by estimation methods based on experimental flight data at center of mass position 30%MAC.

	Absolute values				Relative values			
Param.	**Est.**	**Tornado**	**AVL**	**Datcom**	**Est.**	**Tornado**	**AVL**	**Datcom**
C_{m0}	−0.1025	−0.0013	0.0266	0.0308	1.00	0.01	−0.26	−0.30
$C_{m\alpha}$	−0.428	−0.979	−0.476	−0.777	1.00	2.29	1.11	1.81
C_{mq}	−25.379	−10.768	−8.992	−8.182	1.00	0.42	0.35	0.32
$C_{m\delta_e}$	−2.077	−1.373	−1.147	−1.328	1.00	0.66	0.55	0.64

Table 4.6: Comparison of a–priori moment parameters and moment parameters obtained by estimation methods based experimental flight data at center of mass position 32%MAC.

	Absolute values				Relative values			
Param.	**Est.**	**Tornado**	**AVL**	**Datcom**	**Est.**	**Tornado**	**AVL**	**Datcom**
C_{m0}	−0.0574	0.0102	0.0376	0.0415	1.00	−0.18	−0.66	−0.72
$C_{m\alpha}$	−0.286	−0.877	−0.389	−0.681	1.00	3.07	1.36	2.38
C_{mq}	−24.324	−10.562	−8.840	−8.047	1.00	0.43	0.36	0.33
$C_{m\delta_e}$	−1.839	−1.362	−1.139	−1.319	1.00	0.74	0.62	0.72

4.6.4 Comparison with other airplane category

The ratios of the a–priori values relative to the values obtained by the estimation methods based experimental flight data on SportStar RTC are compared the correction factor of the a–priori values and wind–tunnel data values for a F–18 Hornet model published by J. Kay et al. [24]. The VLM (Vortex Lattice Method), used by J. Kay et al., is the underlaying theory in Tornado and AVL software packages.

The relative values of the investigated longitudinal motion flight parameters are given in Table 4.7.

The differences between the correction factors of the Evektor SportStar RTC and F–18 Hornet models are minor for the lift flight parameters, but higher for the pitch moment parameters.

Table 4.7: Comparison of relative values of low subsonic flight parameters between SportStar RTC and F–18 Hornet.

	SportStar RTC				F–18 Hornet		
Parameter	**Est.**	**Tornado**	**AVL**	**Datcom**	**Data**	**VLM**	**Datcom**
C_{D0}	1.00	0.29	0.48	—	—	—	—
$C_{D\alpha}$	1.00	0.34	—	0.52	—	—	—
C_{L0}	1.00	1.15	1.17	0.87	—	—	—
$C_{L\alpha}$	1.00	0.98	0.96	0.98	1.00	0.93	0.86
$C_{L\delta_e}$	1.00	1.09	0.93	1.02	1.00	0.89	0.84
C_{m0}	1.00	−0.18	−0.66	−0.72	—	—	—
$C_{m\alpha}$	1.00	3.07	1.36	2.38	1.00	0.90	0.95
C_{mq}	1.00	0.43	0.36	0.33	1.00	1.25	0.90
$C_{m\delta_e}$	1.00	0.74	0.62	0.72	1.00	0.97	0.89

5. Conclusion and future work

The objectives of this thesis were to study the theory of the flight data acquisition and flight parameter estimation; to select and implement algorithms suitable for flight parameters estimation of a light airplane. These objectives were met and the author identified the flight parameters of the investigated experimental light airplane.

All flight parameters of the experimental airplane which were estimated based on the measured flight test data fall within the presented limits. For the purposes of the flight parameter estimation, the author used the Equation Error Method, Output Error Method and Recursive Least–Squares methods. The force coefficients containing the longitudinal motion exhibit linear character in the investigated region of the flight envelope. The flight envelope was limited to conditions, in terms of altitudes, airspeed and position of center of mass, as consulted with the airplane manufacturer. Using the model validation process, the author have proved, that the simulated flight data based on the estimated flight parameters sufficiently corresponds to the measured flight data. Therefore, the estimated flight parameters sufficiently describe the airplane aerodynamics and the created model is sufficiently accurate. The flight parameters, the author estimated in this thesis can be used to build a high fidelity flight simulator, which will be able to match the behavior of the real airplane more precisely and therefore improve the airplane pilot training.

The lift based flight parameters have a good a–priori prediction ranging within $[87\%, 117\%]$ of the estimated flight parameters. The relative values of the drag based flight parameters range within $[29\%, 52\%]$ of the estimated flight parameters, which points to a weak spot of the a–priori data sources. The differences between the correction factors of the Evektor SportStar RTC and F–18 Hornet models are minor for the lift flight parameters, but higher for the pitch moment parameters. The presented correction factors are useful during the development phase of a new airplane to conservatively predict its aerodynamic characteristics. The resultant correction factors for the presented computational tools can be applied in the design of a similar category of airplanes, which can lower the expenses of the development cycle. The possible direction of further research is the estimation of the flight parameters for the lateral–directional motion.

The presented contributions were published in international conferences (mostly AIAA and DASC conferences), and these papers were cited several times (see attached List of authors publications and research activities).

Bibliography

1. ALLERTON, David. *Principles of Flight Simulation (AIAA Education Series)*. American Institute of Aeronautics and Astronautics, 2009. ISBN 978-1-60086-703-3.
2. ANSI/AIAA. *Recommended Practice for Atmospheric and Space Flight Vehicle Coordinate Systems*. Washington, DC: American Institute of Aeronautics and Astronautics, 1992. R-004-1992. ISBN 0930403827. Recommendation Practice.
3. ANTSAKLIS, Panos J; MICHEL, Anthony N. *A Linear Systems Primer*. Birkhäuser, 2010. ISBN 0817644601.
4. BD SENSORS S.R.O. *BD SENSORS – Snímače Tlaku* [online] [visited on 2016-08-06]. Available from: http://www.bdsensors.cz.
5. BLOMBERG, H.; YLINEN, R. *Algebraic theory for multivariable linear systems, Volume 166 (Mathematics in Science and Engineering)*. Academic Press, 1983. ISBN 0121071502.
6. BRP-POWERTRAIN. *Operator's Manual For Rotax® Engine Type 912 Series*. Gunskirchen, Austria: BRP-Powertrain GmbH & Co KG., 2010. OM-912. Manual.
7. CHATFIELD, A. *Fundamentals of High Accuracy Inertial Navigation (Progress in Astronautics and Aeronautics)*. American Institute of Aeronautics and Astronautics, 1997. ISBN 1-56347-243-0.
8. CHEN, Ben M.; LIN, Zongli; SHAMASH, Yacov. *Linear Systems Theory: A Structural Decomposition Approach (Control Engineering)*. Birkhäuser, 2004. ISBN 0817637796.
9. CHUDÝ, Peter; DITTRICH, Petr; VLK, Jan. *Dynamický model letounu: Dynamický model letounu kategorie ULL/LSA*. Brno, Czech Republic: Vysoké učení technické v Brně, 2011. AWDM 2.2011. Technical report.
10. DRELA, Mark; YOUNGREN, Harold. *AVL* [online] [visited on 2016-08-06]. Available from: http://web.mit.edu/drela/Public/web/avl/.
11. ETKIN, Bernard; REID, Lloyd Duff. *Dynamics of Flight: Stability and Control*. Wiley, 1995. ISBN 0-471-03418-5.
12. EVEKTOR. *SportStar RTC – Evektor* [online] [visited on 2016-07-04]. Available from: http://www.evektor.cz/cz/sportstar-rtc.
13. FLOSCAN INSTRUMENT CO., INC. *FloScan Aircraft Flow Transducers* [online] [visited on 2016-08-06]. Available from: http://www.floscan.com/html/blue/aviation.php.
14. FRANKLIN, Gene F.; POWELL, J. David; WORKMAN, Michael L. *Digital Control of Dynamic Systems*. Addison-Wesley, 1998. ISBN 0-201-33153-0.
15. GOYER, Robert. *LSA Safety Picture Emerging* [online]. Winter Park, FL: Bonnier Corporation, 2009 [visited on 2016-08-23]. Available from: http://www.flyingmag.com/pilot-reports/lsa/sport/lsa-safety-picture-emerging.
16. GRANGER, Robert A. *Fluid Mechanics (Dover Books on Physics)*. Dover Publications, 1995. ISBN 0486683567.
17. HANAVAN, Ernest P. *A Mathematical Model Of The Human Body*. Wright-Patterson Air Force Base, OH: Aerospace Medical Research Laboratories, 1964. TR-64-102. AMRL.

18. HOTTINGER BALDWIN MESSTECHNIK GMBH. *HBM Test and Measurement* [online] [visited on 2016-08-06]. Available from: https://www.hbm.com.

19. IEEE. *IEEE Standard for Inertial Systems Terminology*. New York, NY: The Institute of Electrical and Electronics Engineers, Inc., 2009. 1559-2009. Standard.

20. ISO. *Quantities and Units—Part 1: General*. Geneva, Switzerland: International Organization for Standardization, 2009. 80000-1:2009. Standard.

21. ISO. *Quantities and Units—Part 2: Mathematical signs and symbols to be used in the natural sciences and technology*. Geneva, Switzerland: International Organization for Standardization, 2009. 80000-2:2009. Standard.

22. JATEGAONKAR, Ravindra V. *Flight Vehicle System Identification (Progress in Astronautics and Aeronautics)*. American Institute of Aeronautics and Astronautics, 2006. ISBN 1-56347-836-6.

23. JOSEFÍK, Miroslav. *Program a Metodiky: Zkoušek projektu „Chytrý autopilot"*. Kunovice, Czech Republic: Evektor spol.s r.o., 2012. RTC.206P.JOS/12. Technical report.

24. KAY, J.; MASON, W. H.; DURHAM, W.; LUTZE, F. Control Authority Assessment in Aircraft Conceptual Design. In: *AIAA Aircraft Design, Systems, and Operations Meeting*. Monterey, CA: American Institute of Aeronautics and Astronautics, 1993, p. 19. No. 3968. Available from DOI: 10.2514/6.1993-3968.

25. KLEIN, Vladislav; MORELLI, Eugene A. *Aircraft System Identification: Theory And Practice*. American Institute of Aeronautics and Astronautics, 2006. ISBN 1-56347-832-3.

26. KUNDU, Ajoy Kumar. *Aircraft Design (Cambridge Aerospace Series)*. Cambridge University Press, 2010. ISBN 978-0-521-88516-4.

27. LEWIS, Frank L.; XIE, Lihua; POPA, Dan. *Optimal and Robust Estimation: With an Introduction to Stochastic Control Theory, Second Edition (Automation and Control Engineering)*. CRC Press, 2007. ISBN 978-1-4200-0829-6.

28. LIVINGSTON, Sadie P.; GRACEY, William. *Tables of Airspeed, Altitude, and Mach Number Based on Latest International Values for Atmospheric Properties and Physical Constants*. Langley Field, VA: National Aeronautions nad Space Administration, 1961. D-822. Technical Note.

29. LOMBAERTS, Thomas. *Fault Tolerant Flight Control – A Physical Model Approach*. Delft, Netherlands, 2010. ISBN 978-90-815443-1-3. PhD thesis. Delft University of Technology, Faculty Aerospace Engineering.

30. MAINE, R. E.; ILIFF, K. W. *Identification Of Dynamic Systems – Applications To Aircraft —Part 1: The Output Error Approach*. Neuilly sur Seine, France: Advisory Group for Aerospace Research and Development, 1986. 300 Vol.3. ISBN 92-835-1540-4. AGARDograph.

31. MATHWORKS. *MATLAB & Simulink* [online] [visited on 2016-08-06]. Available from: https://www.mathworks.com/products/matlab.html.

32. MELIN, Tomas. *A Vortex Lattice MATLAB Implementation for Linear Aerodynamic Wing Applications*. Stockholm, Sweden, 2000.

33. NATIONAL INSTRUMENTS CORPORATION. *LabVIEW System Design Software* [online] [visited on 2016-08-06]. Available from: http://www.ni.com/labview/.

34. NATIONAL INSTRUMENTS CORPORATION. *The CompactRIO Platform* [online] [visited on 2016-08-06]. Available from: http://www.ni.com/compactrio/.
35. PENNY&GILES. *SRS280 – Sealed Rotary Sensor* [online] [visited on 2016-08-06]. Available from: http://www.cw-industrialgroup.com/Products/Sensors/Rotary-Hall-Effect-Position-Sensors/Sealed-Rotary-Sensor-SRS280.aspx.
36. RAOL, Jitendra R.; SINGH, Jatinder. *Flight Mechanics Modeling and Analysis*. CRC Press, 2008. ISBN 978-1-4200-6753-8.
37. RED LION CONTROLS, INC. *Red Lion. Connect. Monitor. Control.* [online] [visited on 2016-08-06]. Available from: http://www.redlion.net.
38. ROGERS, Robert M. *Applied Mathematics in Integrated Navigation Systems, Third Edition (AIAA Education)*. American Institute of Aeronautics and Astronautics, 2007. ISBN 1-56347-927-3.
39. SPACEAGE CONTROL. *Data Sheet - 100400 Mini Air Data Boom* [online] [visited on 2016-08-04]. Available from: http://spaceagecontrol.com/Main/S002c.
40. STENGEL, Robert F. *Stochastic Optimal Control: Theory and Application*. Wiley-Interscience, 1986. ISBN 0-471-86462-5.
41. STEVENS, Brian L.; LEWIS, Frank L. *Aircraft Control and Simulation*. Wiley-Interscience, 2003. ISBN 0-471-37145-9.
42. STOCK FLIGHT SYSTEMS. *IFNS* [online] [visited on 2016-08-06]. Available from: http://www.stockflightsystems.com/ifns.html.
43. TEWARI, Ashish. *Atmospheric and Space Flight Dynamics: Modeling and Simulation with MATLAB® and Simulink® (Modeling and Simulation in Science, Engineering and Technology)*. Birkhäuser, 2007. ISBN 0-8176-4373-7.
44. ÚŘAD PRO CIVILNÍ LETECTVÍ. *Přehled vydaných Oprávnění k provádění zkoušek letecké techniky podle Postupů CAA-TI-012-4/99* [online] [visited on 2016-08-06]. Available from: http://www.caa.cz/letadla/prehled-vydanych-opravneni-k-provadeni-zkousek?highlightWords=l-3-060.
45. USAF TEST PILOT SCHOOL. *Flying Qualities Textbook, Volume 2*. Edwards AFB, CA: USAF, 1986. USAF-TPS-CUR-86-02.
46. VISHAY PRECISION GROUP. *General Purpose Strain Gages 250UN* [online] [visited on 2016-08-06]. Available from: http://www.vishaypg.com/micro-measurements/list/product-11298/.
47. VISSER, Cornelis Coenraad de. *Global Nonlinear Model Identification with Multivariate Splines – Application to Aerodynamic Model Identification of the Cessna Citation II*. Delft, Netherlands, 2011. ISBN 978-90-8570-770-7. PhD thesis. Delft University of Technology, Faculty Aerospace Engineering.
48. WAGUESPACK, Curtis. *Mastering Autodesk Inventor 2015 and Autodesk Inventor LT 2015: Autodesk Official Press*. Sybex, 2014. ISBN 978-1-118-86213-1.
49. WILLIAMS, John E.; VUKELICH, Steven R. *The USAF Stability And Control Digital Datcom*. Wright–Patterson Air Force Base, OH, 1979. TR-679-3032. AFFDL.
50. XSENS. *MTi-G GPS-aided AHRS* [online] [visited on 2016-08-04]. Available from: https://www.xsens.com/products/mti-g/.

51. YECHOUT, Thomas R.; MORRIS, Steven L.; BOSSERT, David E.; HALLGREN, Wayne F. *Introduction to Aircraft Flight Mechanics: Performance, Static Stability, Dynamic Stability, and Classical Feedback Control (AIAA Education Series)*. American Institute of Aeronautics & Astronautics, 2003. ISBN 978-1-56347-577-1.